Investigation of Electrochemical and Material Properties of TiO_2 Nanostructures Generated by Pulsed Laser Ablation

by

Amirhossein Gholami

A thesis submitted to the
School of Graduate and Postdoctoral Studies in partial
fulfillment of the requirements for the degree of

Master of Applied Science

in

Mechanical Engineering

Faculty of Engineering and Applied Science

University of Ontario Institute of Technology (Ontario Tech University)

Oshawa, Ontario, Canada

April 2022

THESIS EXAMINATION INFORMATION

Submitted by: **Amirhossein Gholami**

Master of Applied Science in **Mechanical Engineering**

Thesis title: Investigation of Electrochemical and Material Properties of TiO_2 Nanostructures Generated by Pulsed Laser Ablation

An oral defense of this thesis took place on April 18, 2022 in front of the following examining committee:

Examining Committee:

Chair of Examining Committee	Dr. Martin Agelin-Chaab
Research Supervisor	Dr. Amirkianoosh Kiani
Examining Committee Member	Dr. Sayyed Ali Hosseini
Thesis Examiner	Dr. Xianke Lin, Ontario Tech University

The above committee determined that the thesis is acceptable in form and content and that a satisfactory knowledge of the field covered by the thesis was demonstrated by the candidate during an oral examination. A signed copy of the Certificate of Approval is available from the School of Graduate and Postdoctoral Studies.

ABSTRACT

The most challenging feature of the supercapacitor is low energy density. The supercapacitor's low energy density can be improved by proposing new materials for electrodes, electrolytes, etc. This thesis presents a new method for fabricating electrodes in a supercapacitor structure. In this method, we use pulsed laser ablation with the theory of increasing the surface area of electrodes. Although this method can be applied in different materials, we use titanium as a low-cost and lightweight material in our experiments. We use electrochemical and physical properties to investigate the effectivity of this method in different ways. In the first phase, we analyzed the electrochemical and physical properties of TiO_2 electrodes by changing one laser parameter. In the second phase, we propose inverse engineering to calculate input parameters to fabricate specific supercapacitors based on machine learning techniques. In the second phase, we compare the result for three different machine learning algorithms then pick one for the inverse engineering structure.

Keywords: supercapacitor; electrode; pulsed laser; machine learning

AUTHOR'S DECLARATION

I hereby declare that this thesis consists of original work of which I have authored. This is a true copy of the thesis, including any required final revisions, as accepted by my examiners.

I authorize the University of Ontario Institute of Technology (Ontario Tech University) to lend this thesis to other institutions or individuals for the purpose of scholarly research. I further authorize University of Ontario Institute of Technology (Ontario Tech University) to reproduce this thesis by photocopying or by other means, in total or in part, at the request of other institutions or individuals for the purpose of scholarly research. I understand that my thesis will be made electronically available to the public.

Amirhossein Gholami

YOUR NAME

ACKNOWLEDGEMENTS

I would like to express my gratitude and appreciation to all those who gave me the possibility to complete this report. Special thanks are due to my supervisor Dr. Amirkianoosh Kiani, whose help, stimulating suggestions, and encouragement helped me in all the fabrication process and in writing this thesis. I also sincerely thanks for the time spent proofreading and correcting my many mistakes.

STATEMENT OF CONTRIBUTIONS

Part of the work described in Chapter 3 and Chapter 4 are either published or under consideration for publication as:

Gholami, A.H, Kiani, A, "Laser-induced nanofibrous titania film electrode: A new approach for energy storage materials", Journal of Energy Storage 31, 101654, 2020 https://doi.org/10.1016/j.est.2020.101654

Gholami, A, Yim, CH, and Kiani, A, "Electrochemical Performance of Titania 3D Nanonetwork Electrodes Induced by Pulse Ionization at Varied Pulse Repetitions", Nanomaterials 11 (5), 1062, 2020 https://doi.org/10.3390/nano11051062

Table of Contents

LIST OF TABLES

LIST OF FIGURES

LIST OF ABBREVIATIONS AND SYMBOLS

SEM	Scanning Elecron Microscope
XRD	X-ray Diffraction
IE	Inverse Engineering
ML	Machine Learning
NN	Neural Network
PEM	Proton Exchange Membrane
EDLC	Electrical Dual Layer Capacitors
EES	Electrochemical Energy Storage
PLA	Pulsed Laser Ablation
CE	Counter Electrode
WE	Working Electrode
RE	Reference Electrode
OM	Optical Microscope
CV	Cyclic Voltammetry
EIS	Electrochemical Impedance Spectroscopy
CCD	Cyclic Charge Discharge
ESR	Equivalent Series Resistance
CCD	Cycle Charge Discharge
PES	Photo-Electrochemical Systems
MCVD	Metalorganic Chemical Vapor Deposition
FWHM	Full With Half Maximum
EOM	Electro-Optical Modulator
SVM	Support Vector Machine
QP	Quadratic Program

Chapter 1. Literature Review

1.1 Introduction

Today's world is developing based on fossil fuel which is on the opposite side of environmental-friendly strategy and economical-balance laws [1]. With decreasing the fossil fuel source, we are facing the increase of extraction cost, which is an excellent reason to think about substituting option [2]. Simultaneously, we need a manageable extra source of energy in addition to fossil fuels to handle a considerable amount of consumption. That means the generation timing is an essential factor that should be considered when going through the new sources [3]. Any development aiming to meet the fundamental demands in transportation, housing, industry, and agriculture require a long term, sustainable, economic, and ethical parameters for the next generation while increasing food security, energy security, and quality of life

Since the beginning of the twentieth century, raw energy has significantly expanded due to population and economic expansion. Furthermore, recurrent quick industrialization and the quest for intelligent technologies necessitate more energy resources than ever before [4]. Consumption has skyrocketed, posing new energy security difficulties and contributing to environmental issues and global warming. The increasing need for energy and the shortage of traditional energy supplies have accelerated research into alternative energy resources and energy storage systems. Electrochemical storage has been acknowledged as one of the most significant inventions in the history of energy storage technologies. Supercapacitors and batteries are two main types of storage devices. The former has the unique benefit of high-powered energy storage capabilities, but it lacks energy. On the other hand, batteries have great energy but low power density, limiting their applicability when fast energy

generations are required. By manufacturing the hybrid device using a single component from each device, the advantages of both devices may be reaped in a single device [5-9].

Energy storage is crucial to today's energy networks [10]. Much energy is now stored in raw or processed hydrocarbons, whether in the form of coal piles or oil and gas reserves. Because energy storage is significantly more efficient, power precursors are stored rather than electricity, generating requirement changes. The only exception is a pumped hydroelectric plant, which may supply a large amount of electricity in a short period and can increase electric system dependability on short notice [11]. The function and form of energy storage are anticipated to alter significantly as energy systems evolve to incorporate low-carbon technologies. Two main tendencies might influence this change. For starters, with intermittent nuclear power and stationary production playing an increasingly important role, the energy supply will become increasingly difficult to match with demand, resulting in imbalances that will increase and dominate over time [12]. Moving away from fossil fuel production implies that most power sources can no longer be stored as hydrocarbons except for flexible gas generation.

Furthermore, if low-carbon power replaces oil and gas for transportation and heat delivery, where demand is highest, the structure of electricity demand will shift dramatically [13]. Electricity is stored during periods of surplus energy supply to fulfill demand in the development of energy storage technology. Other storage strategies, for example, might help the energy system in other sectors by storing surplus electricity, such as heat or hydrogen, for use in other industries. The utilization of energy storage will only trigger a revolution in the transition to a low-carbon civilization. Fuel cells that use liquid fuels, such as methanol, have a large energy storage capacity, but their power output is restricted. Li-

oxygen batteries can have a high energy density but a poor power output [15]. As a result, their performance is only optimal for continuous production, and their lack of reaction time necessitates using another storage such as batteries. As demonstrated in Fig. 1.1, none of the storage methods can compete with gasoline's efficiency.

There are two main forms of electric power storage: batteries and condensers. Electric energy is stored in condensers as a surface charge, similar to how chemical energy is kept in a battery. Chemical reactions occur across the whole solid mass of the battery, allowing the reacting process to fill the generation and then be discharged. It must be repeated tens of times to produce a commercially viable rechargeable battery. Nonetheless, a considerable portion of the surface area is used for a capacitor (the storage capacity is

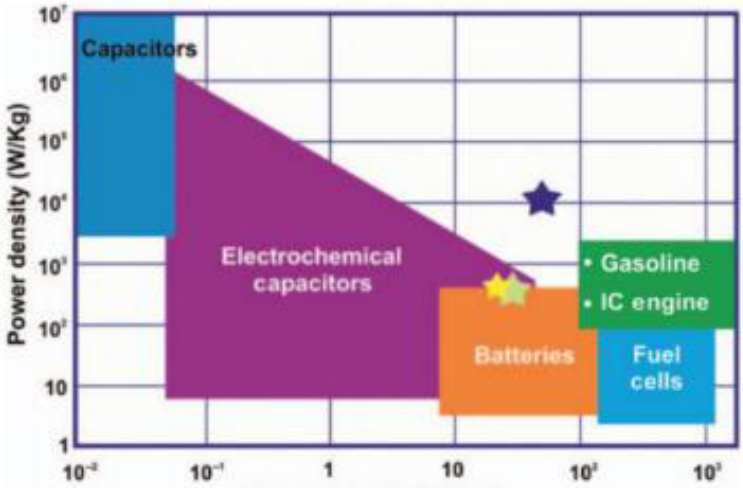

Figure 1.1 Comparison of Energy Storage, Figure reproduced with permission from ref [16], Elsevier 5294260703199

directly proportional to the surface area). Because there is no doubt about the structural integrity of a capacitor component, the pure capacitor may be charged and discharged several million times without significant generation loss. In contrast, battery chemical reactions cannot always be reversed owing to structural material alterations [17].

Supercapacitors cross between the two, incorporating non-faradaic load and specific faradic responses. As illustrated schematically in Fig. 1.2, batteries and supercapacitors have two electrodes, the anode, and the cathode. The cathode is the electrode to which electrons are directed as they pass through the operational circuit. The anode is the electrode via which electrons flow in an external working circuit. To balance the electron stream, ions typically move from anode to cathode through the battery's electrolyte. A single ion, rather than electrons, escapes from a liquid or solid electrolyte. A porous separator is inserted between the two electrodes to prevent them from contacting one other.

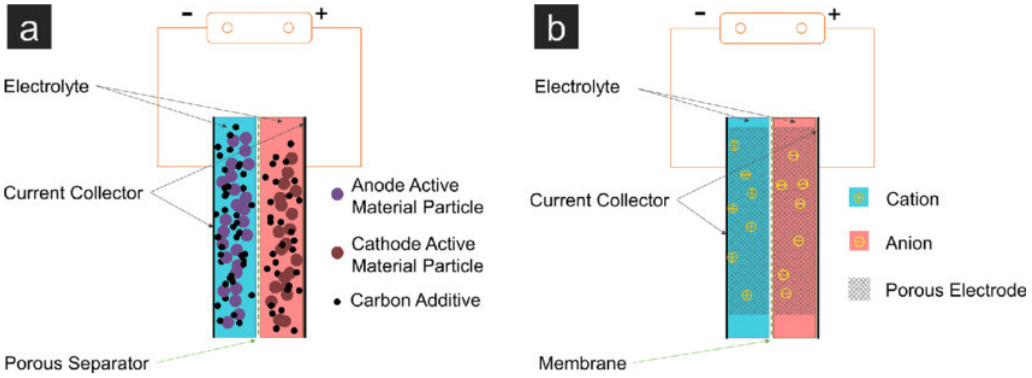

Figure 1.2. Schematic of (a) Battery and (b) Supercapacitor [21]

Ionic normally migrate from anode to cathode via the electrolyte in a battery [18, 19]. The first thermodynamic law asserts that total energy in a closed system is fixed and that energy cannot be created or destroyed (It can only be converted from one kind to another). This fundamental concept underpins the transformation and storage of nearly all forms of energy [20]. As a result, the majority of storage techniques fall into four main categories: mechanical energy storage, chemical energy stockpiling, electrochemical energy storage, and electric energy storage. The maximum quantity of electrical energy that a storage system can extract is provided by [22]:

$$G = H - TS \qquad 1.1$$

G denotes Gibbs' free energy or enthalpy. *T* is the temperature, and S is the entropy. In other words, G indicates the highest amount of energy that may be used to do mechanical or electrical work. Potential, E_p, and kinetic energy storage express themselves in mechanical energy storage, such as pumped hydro. Energetic units can be represented by:

$$E_{pot} = fd \qquad 1.2$$

$$E_{kin} = \left(\frac{1}{2}\right) mv^2 \qquad 1.3$$

In this equation, *f* denotes force, *d* indicates distance, *m* is mass, and *v* represents the velocity. Kinetic energy is defined in a similar way for a spinning body, such as a flywheel or a wind turbine, by,

$$E_{kin} = \left(\frac{1}{2}\right) I\omega^2 \qquad 1.4$$

Where *I* signify the moment of inertia and *w* denotes the spinning system's angular velocity. In other words, stored energy grows in proportion to the system's inertia and the square of its rotational velocity. The body moment of inertia with mass (*m*), radius (*r*), length (*l*), and density (ρ) may be calculated as follows:

$$I = \left(\frac{1}{2}\right) mr^2 or = \left(\frac{1}{2}\right) \rho l \pi r^4 \qquad 1.5$$

As a result, high-density materials with a significant radius aid in the storage of more energy. Eq. (1.5) may also be represented in terms of mechanical energy storage in flywheels [24].

$$E_{kin} = \frac{\sigma_m s}{\rho} \qquad 1.6$$

Maximum stress is denoted by σ_m , the shape factor is *s*, and material density is ρ. It is conceivable to reach storage capacities larger than 200 kJ per kilogram of flywheel mass with current flywheels comprised of reinforced high-strength carbon fibers. The gas law (PV = nRT) is used for compressed air storage in salt caverns or subterranean aquifers, and the available work, *w*, is supplied by *PdV* integrated over the incremental volume change (*dV*)

$$q = \rho C_p V \Delta T \qquad 1.7$$

The total energy maintained in the case of a phase shift in the thermal energy processing or substance must account for the latent heat associated with that transformation [25]. Chemical storage is based on the energy storage of chemical bonds in fuels, which are essentially solid and afford very high energy densities [26]. Nonetheless, chemical manufacturing frequently necessitates the utilization of electric or thermal power. In the case of electrical batteries or electrochemical interfaces, electrochemical processing systems are based on the containment of electrical condensers and supercapacitors or the chemical bonding of fuel cells [27]. The ratios of (AG/AH) characterize the inherently high efficiency of electrical energy processing. High efficiency is provided via electrochemical energy storage. Finally, electric and magnetic power storage may be implemented.

1.2 Electrochemical Energy Storage Systems and Materials [28]

The fundamental working theory of electrochemical and photoelectrochemical processes (photovoltaic membrane) contains three critical process steps: charging separation (or

ionization), charged species transport, and charging recombination. This fundamental idea governs the operation of a wide range of devices such as photochemical and photovoltaic structures, batteries, fuel cells, supercapacitors, and electrolytes. On the other hand, their working conceptions necessitate diverse systems, with interfaces playing a critical role. Because batteries store charges in the electrodes, fuel cells and battery charge flows are contained in the gas, which is pushed to the electrode's surface from outside [29].

Supercapacitors charge either at the electrode/electrolyte interface in the double-layer electric or as redox-surface response opt-outs. PEMFC, supercapacitors, and batteries, for example, operate at normal temperatures, whereas sodium or molten carbonate and solid oxide fuel cells operate at high temperatures. In other words, the product requirements for each electrochemical storage system are distinct, and several have been thoroughly examined elsewhere [30-32]. A recent review paper [33] describes the fundamental and operational ideas of batteries, fuel cells, and supercapacitors. The essential idea behind electrochemical energy storage is the reciprocity between turning the chemical energy stored in energy bonds into electricity and utilizing electric power by reversibly synthesizing chemicals or energy. The Gibbs free energy change (AC) of the electrically neutral species at the electrodes participating in the chemical reaction is the driving force for this conversion.

$$A + B = C\ \Delta G\left(\frac{kJ}{mole}\right) \qquad 1.8$$

If reactants A and B are exposed to a purely chemical reaction, as in Eq. (1.8), or an electrochemical reaction including the transfer of ions and electrons across the cell, the free change in energy is the same. Because these species are electrically charged, the

electrostatic energy transferred across by a mole of such species is given by ZEF_i, where *Fi* is Faraday's constant, *Z* is the transporting species' charge number, and *E* is the cell voltage. Under open-circuit circumstances, the cell voltage is proportional to the change in Gibbs free energy.

In other words, the potential chemical difference between neutral species at the electrodes explains the fundamental force that drives an electrochemical cell to produce an electrically neutral product. *C* is formed as a result of a chemical reaction between two electrically neutral reactants (A and B). The systems include critical features for electrical processing, such as two specialized electrode bodies separated by an ionically conducting yet electrically segregated "electrolyte." Electrodes with high electronic conductivity, stability, and catalytic activity are preferably made from available and inexpensive materials.

It is worth mentioning that batteries, electric condensers, and supercapacitors combine specific energy and specific power with appropriate material selection. Nonetheless, material selection determines energy efficiency, which is connected to cellular materials' kinetic and transport properties. Many people will profit much from such decoupling. The volumetric densities of electrical storage devices are also significant. Volume is especially crucial when it comes to driving storage and mobile applications. The focus is on whether Li-ion batteries or fuel cells will eventually supplant mobile applications and, more particularly, which in the transportation market will be used [34].

1.3 Energy Storage Development [35-42]

Mechanical, thermal, electrical, magnetic, and chemical energy storage are the five basic types of energy storage systems [21]. These include physical, chemical, and

electromagnetic technologies, such as hydrogen energy storage. Each technology has its own set of characteristics that make it suitable for various applications. Until 2016, the world's energy storage technology was dominated by pumped hydro storage (Fig. 1.5).

Pumped hydro growth has gone up since 2015, with an annual increase of barely 1.8 percent. In terms of total global capacity, molten salt thermal energy storage comes in second place. Electrochemical energy storage capability ranks third, with the most development, with a total capability of 1769.9 MW, up by %56 from the previous year. Among electrochemical power storage systems, lithium-ion power storage has the most installed capacity, accounting for % 65 of the total capacity. This number has increased by %89 since 2015.

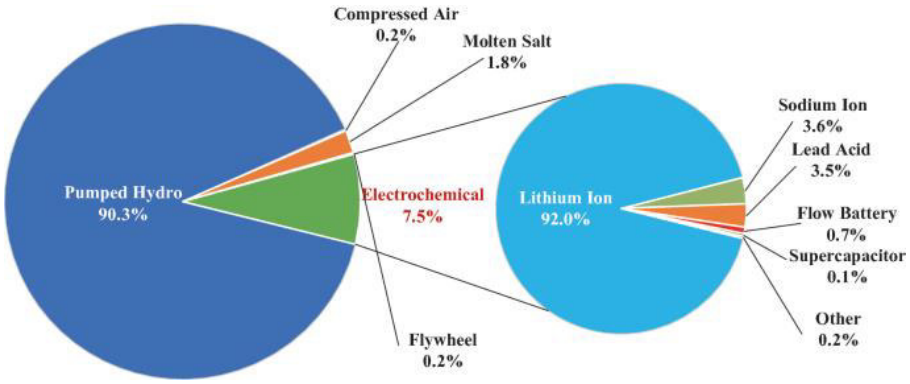

Figure 1.3 Electrochemical Storage Categorization [43]

Figure 1.3 depicts a schematic illustration of energy storage methods. The mechanical energy storage technique largely involves the storage of pumped gas, compressed air storage, and flywheel control. Pumped storage is the most established technology, with great capability, long service life, and cheap unit cost. However, geographical constraints limit the growth of the pumped-storage power plant, longer construction duration, and the overall investment is significant. Compressed air energy storage advantages include large

capacity, long-running period, long service life, etc. In addition, it may provide combined heat, cold, and power by converting compressed air into alternative energy. Despite its low efficacy, the system is complex, and the air storage tunnel placement need high mining [44]. The benefits of flywheel energy storage include high effectiveness, quick response, long service life, lower operating and maintenance requirements, excellent stability, short building time, low footprint, and no pollution; however, the energy density is low, and it is easy to self-discharge, making it only suitable for short-term applications [45].

Heat storage is divided into two types [46, 47]: sensible heat storage and latent heat storage. Water is employed as a way for heat storage, and by increasing the temperature of the heat storage material, the goal of the sensible material may be completed. Solar and thermal power plants use latent heat storage, which uses regenerative materials. The photothermal system generates both the needed heat and power. In the winter, for example, a solar-only system is insufficient.

As a result, thermal (heat) energy enters the scene. The power storage efficacy of the heat storage system may reach %95 [48], while the cost of storing huge batteries is only approximately 1/30 $/kw. The concentrated solar thermal power facility is now used as a research hotspot for molten salt storage technology. Some of the key benefits are cost savings, increased heat output, and the fact that it is safe and secure. These systems are available for purchase in Europe and North America [50]. However, the concerns remain apparent in its actual execution, with one of its flaws being its corrosive character. Furthermore, the high molten salt solidification temperature makes it easy to scrap machinery.

	Technologies	Characteristics
Physical Storage	Pumped Hydro Compressed air (supercritical CAES) Flywheel	Uses water/air as a storage medium No chemical change Mechanical-electric energy
Chemical Storage	Lead-acid battery Li-ion battery Flow battery (Vanadium, Zn-Br) Na-S battery	Uses chemicals as storage medium battery charges/discharges with chemical change/valence change
E&M Storage	Supercapacitor	Fast response, can release large amounts of electric power in short times, the high number of cycles
Other storage	Fuel cell Metal-air battery	Does not possess "charging" characteristic

Figure 1.4 Energy Storage Technologies, Figure reproduced with permission from ref [51], Elsevier 5294300755932

Several methods use chemically storing electrical energy, including lead-acid batteries, lithium-ion batteries, sodium-sulfur batteries, and redox flow batteries. Some of the advantages of traditional batteries were that they were inexpensive and straightforward to use, but they had limitations such as smaller capacitances and less significant power density, lower energy density, shorter life cycle, and pollution. In recent years, Japan, the United States, and other countries have been committed to producing more advanced lead-acid batteries and numerous types of batteries, such as lead-carbon batteries, super batteries, and so on. Lithium-based batteries include lithium-iron-phosphate (Li-Fe-P) batteries and titanium-lithium batteries (Li-Ti). Li-nickel-manganese-cobalt (Li-NMC) batteries are used in the power industries. The importance of Li-Fe-P has improved the stability and life cycle. Li-Ti is more cost-effective, with guaranteed safety, a longer life cycle, and an acceptable charge and discharge process.

The Li-NMC batteries are responsible for the increased energy density and power density. Some of the disadvantages of Li-NMC batteries are their high cost and limited availability of cobalt salt. There are currently two types of redox flow batteries under investigation: vanadium and bromine-zinc redox flow batteries. The vanadium redox flow battery has a long cycle life and a long life; however, it has a low energy and power density and a slow response. Zinc-bromine flow batteries have high energy, low cost, and regular deep discharge rate, but they also have a better rate of self-discharge caused by a complex electrode reaction. The sodium battery has several benefits, including high energy density, excellent performance, longer lifetime, etc. It has matured into a well-developed, commercially viable electrochemical energy storage technology at the MW level. However, it uses the combustible metal sodium and operates at high temperatures (300°C-350°C), posing a security issue [52].

Electromagnetic energy storage, which stores energy in an electrical field, is used in electromagnetic storage systems. The benefits of ultracapacitors are that they discharge much quicker than electrochemical battery-storage discharges and alter power densities faster than battery-driven power densities without relying on chemical processes. They can also withstand one million charge and discharge cycles and have an output of roughly %100. Ultracapacitors are smaller and lighter than batteries [53], and no harmful chemicals or metals are required. Ultracapacitors are not intended for long-term usage but rather for extremely brief energy bursts. Ultracapacitors can also be used to enable renewables by firming power generation. Current research has also been conducted to supply wind turbines with the power they require to modify their pitch or angle to help collect wind energy. As a holding gear hybrid of longer-lasting battery schemes, ultracapacitors are

projected to give short-term power before the battery system joins. The extra energy supply can swiftly refill them. Electromagnetic energy storage is primarily accomplished using supercapacitors and superconductive magnets [54]. The supercapacitor has the advantages of high energy density, rapid reaction, high efficacy, long cycle life, minimal maintenance, a broad range of working temperatures, etc.

On the other hand, the supercapacitor is suitable for usage with other energy storage methods due to its low power density [55]. The charge/discharge speed of a supercapacitor is significant because it has benefits such as high power density and quick response, high efficiency in energy conversion, long lifetime, and so on, making it suited for high energy requirements. However, the expensive cost, low energy density, and rigorous maintenance are disadvantages [56].

Chemical energy storage is secondary hydrogen, or synthetic gas fuel carrier that electrolyzes hydrogen and may also be synthesized with carbon dioxide into natural gas (i.e., methane). This green technique might lead to more than 100 GWh of large-scale energy storage without polluting the environment. On the other hand, the conversion efficiency issue is only %40 -%50, and there is a high cost needing a significant investment and low security [57]. Many countries have also shown hydrogen energy storage devices, although fuel cells are the primary use of hydrogen.

The proton exchange membrane (PEM) in the fuel cell is extensively employed as a backup energy source, increasing the use of renewable energy in the electrical, thermal, transportation, and other sectors. The fundamental goal of introducing renewable energy and hydrogen as the principal energy source today is to enhance the cost-efficacy and life span [58].

To conclude this section, different storage options are available. Fuel cells, like batteries, use an electrochemical process to give energy, but they differ in that electricity is generated using a hydrogen-containing fuel that combines with oxygen, which is usually obtained from the air. Fuel cells can continuously produce energy as long as they have both a fuel and an air supply; hence they do not fit into the standard battery charging and recharging cycles. Metal-air batteries, which have a cathode-like anode consisting of metal and air, also promise various metal technology.

1.4 Electrochemical Energy Storage

Electrical dual-layer capacitors (EDLCs) are supercapacitors with a high specific power density that may be charged and discharged up to 10 times per second without power decrement [59]. EDLCs store electrical energy by adsorption of physical ionic type on the interior surfaces of high porosity electrodes rather than electrochemical processes. In the meanwhile, recharging the supercapacitors necessitates a low energy density. Compared to batteries [60], EDLCs offer additional benefits due to their quick charging, high power densities, and longer cycle life. The charging and discharging of almost 1000-2000 cycles of electrochemical double-layer electrodes at a very porous surface supports the operating concept of an ideal EDLC. Over the last few decades, various materials have been proposed for supercapacitors' electrodes. Complex morphology, high micropore architecture, well-adjustable pore size distributions, and utility, such as porous material electrodes, were essential aspects of these materials. Many materials have been tested as EDLC elements, including carbon, metal oxides, conducting polymers, and synthetic polymers. Despite this, carbon electrodes with a wide surface area have been employed, and most porous electrodes are constructed of carbon. The key characteristics that attract porous carbons for

practical applications are ease of processing, nontoxicity, chemical stability, reduced density, more significant surface area, excellent electrical conductivity, and comparably inexpensive materials. Electrolyte selection is also critical for improving EDLC performance. Room-temperature ionic liquids are often utilized as working electrolytes because of their large potential windows, thermal stability, and nonvolatility. The simplicity of the models related to the shape of adjustable pores and the interaction of electrolyte and electrode is used in theoretical modeling for the research of EDLCs. Three types of electrode designs are commonly employed in EDLC academic research. Several EDLC models were employed in the study, including flat surfaces, cylindrical pores with concave internal surfaces, and cylindrical particles with convex exterior surfaces and spherical surfaces. Electrochemical energy storage (EES) engineering for high energy density applications is the subject of some research. In both present and near-future applications, storage with high energy and high-power densities for the same material are becoming increasingly necessary. Pseudocapacitors are a faradaic redox cycle on or near the surface, allowing for high energy density at high load discharge rates.

EES is a type of energy storage system that is commonly utilized to save and generate electricity. It is increasingly employed in the fabrication of portable gadgets. In the form of batteries and electrochemical capacitors, it may also be used to electrify the transportation industry. Over the next few decades, global energy demand is predicted to rise. EES technologies are coupled with the power grid and renewable energy sources such as solar and wind for electric grid power. Although there are several applications for EES, these devices must overcome a number of obstacles, and research should focus on developing better materials for energy storage. Basically, abundant and harmless materials

should be employed for energy storage fabrication, which would lower prices and increase the reliability of EES devices.

1.4.1 Electrochemical Capacitors [62-66]

The process of charge/discharge is very reversible, and the life cycle is nearly infinite in classic capacitors. On the other hand, Pseudocapacitors do not store energy in EDLCs via the electrical double layer. Fast oxidation-reduction processes (redox) and possible interaction of electrodes save energy. The electrode's fabrication material and the electrolyte influence the electrochemical condenser's performance. (1) carbon-based materials, (2) metal transition oxides, and (3) conductive polymers are the three basic electrode material categories employed in ECs. Organic electrolytes, ionic acid, and aqueous electrolytes are the three electrolyte compounds for ECs. The output of ECs resembles that of several electrical storage devices. The energy and power densities of Ragone's map are shown in Fig. 1.3. The fuel cells and batteries imply very high energy densities compared to capacitors. On the other hand, Capacitors have poor energy densities due to their material loading capabilities. Batteries and fuel cells have a high energy density due to their slower kinetic processes and low power density.

EC devices have attracted a lot of attention since they have the unique characteristics of a fast charging-discharging rate and a long-life lifetime. In EC devices, charging and discharging may happen in seconds. Other energy storage technologies have lower power densities than this. General Electric presented the first EC-related patent in 1957. They have since been employed in various applications, including power supply and storage, backup power, and power quality enhancement.

Ionic adsorption on the electrode surface allows EDLCs to be kept in energy without faradaic reactions. During the charging and discharging operation, the arrangement of the charges inside the double layer of Helmholtz causes a displacement current. The materials swiftly respond to potential changes and physical reactions. As a result, it can supply energy fast. However, the amount of stored energy is limited, and it is significantly smaller than that of pseudocapacitors and batteries. The EDL capacitance is described as follows

$$C_{dl} = \frac{Q}{V} = \frac{\varepsilon_0 \varepsilon_r A}{d} \qquad 1.9$$

where C_{dl} is the EDL capacitance of a single electrode. Q denotes the total charge transferred at potential V, ε_r is the electrolyte's dielectric constant, ε_0 is the vacuum's dielectric constant, d is the charge separation distance, and A is the electrode surface area. Eq. 2.2 may be used to construct the following equation defining the response current I for EDLCs when C_{dl} is constant. The following equation describes the response current I, which can be defined from Eq. 2.2

$$I = \frac{dQ}{dt} = C_{dl} \frac{dV}{dt} \qquad 1.10$$

where *t* is the time, it takes to charge. The relationship may be represented if the applied voltage V fluctuates linearly with time *t*, that is, $V = V_0 + vt$ (where V_0 is the starting voltage and v is the sweep rate (Vs^{-1} or mVs^{-1}')). The relationship can be described as:

$$I = C_{dl} v \qquad 1.11$$

The magnitude of current changes linearly with the sweep rate, according to Eq. (1.10). A well-defined plot of rectangular current voltage or cyclic voltammogram is feasible using

various sweep speeds. When the ES is charged or discharged with a continuous current, the voltage increases (charge) or decreases (discharge).

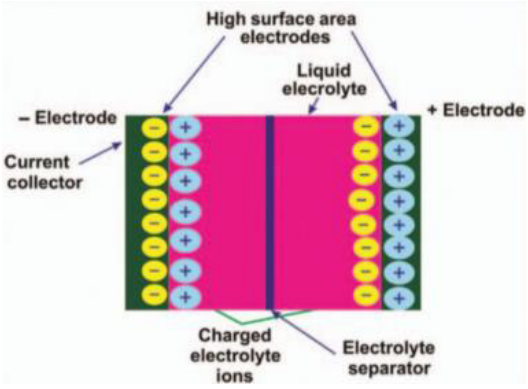

Figure 1.5 Electrochemical Capacitor, Figure reproduced with permission from ref [67], Elsevier 5294310709483

In that instance, a triangular charge/discharge curve is expected to be formed. Over the last few years, much research has gone into understanding and modeling electrode materials for energy storage applications. Carbon-based materials, such as activated carbon and graphene carbon nanotubes, are employed as EDLC supercapacitors. The electrode's surface area, functional surface state, pore texture, pore distribution, and many carbon layers are crucial variables in this scenario. However, by combining carbon pore sizes to electrolyte ion sizes and carbon surface functionalization using oxygen or increasing oxygen content, using redox-active species-based electrolytes [36], and designing new forms of ionic iodide or cooping [40,41], the energy efficiency of EDLC can be improved. Because of their inherent drawbacks, the use of EDLC supercapacitors at more significant sizes in high-energy-density devices is still limited.

1.4.2 Electrical double-layer capacitor

An electrolyte separates two electrodes into a single cell. An electrostatic charge is stored at the contact between an electrode and an electrolyte. Opposite directions are inserted on

two constant levels to explain the name's origin. As illustrated in Fig. 1.6, one pair is on the electrode, and the other is on the electrolyte.

There is no dielectric separator in electrostatic and electrolytic capacitors. However, the operating voltage is limited by the electrolyte's stability. A potential difference arises throughout the double layer. The distance between charges is only a few Angstroms. As electrodes, materials with a wide surface area are used and form Eq (1.12)

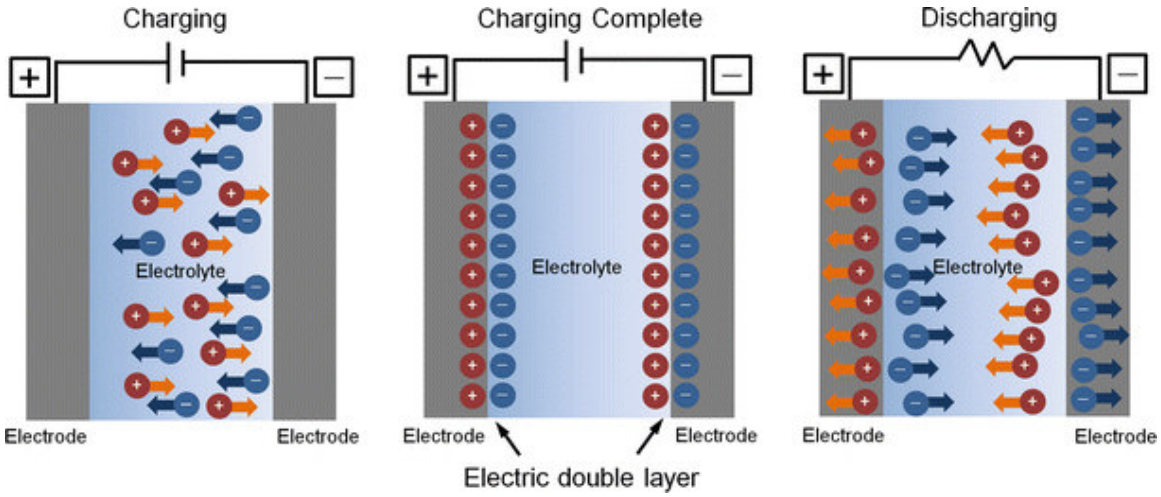

Figure 1.6 EDLC shown with the charge separation at both electrodes [68]

$$C = \frac{\varepsilon_0 A}{d} \qquad 1.12$$

The total value is little because the surface area A is large and the distance d is tiny. When the packed EDLC is fully charged and discharged, the charging process is seen in Figure 1.6.

When a voltage is generated between two electrodes, electrolyte ions with opposite polarity are absorbed on the electrodes. As a result, double layers are formed on both electrodes. When the charge is applied, the voltage source is replaced, and the ions return to the electrolyte. Aqueous or organic electrolytes can be used in this structure. Using an

equivalent electrical circuit, Figure 1.7 shows the voltage distribution through a charged EDLC. Both electrodes contribute to C_1 and C_2 in the presence of a charge-separation capacitor, as shown in Figure 1.7, when they are coupled in a series connection, felt here due to the presence of collectors R_1 and R_2. There is resistance. Also, the internal R_i resistance is due to ions' movement inside the electrolyte. Using Fig. 1.7, the capacitance behavior of the double layer may be described.

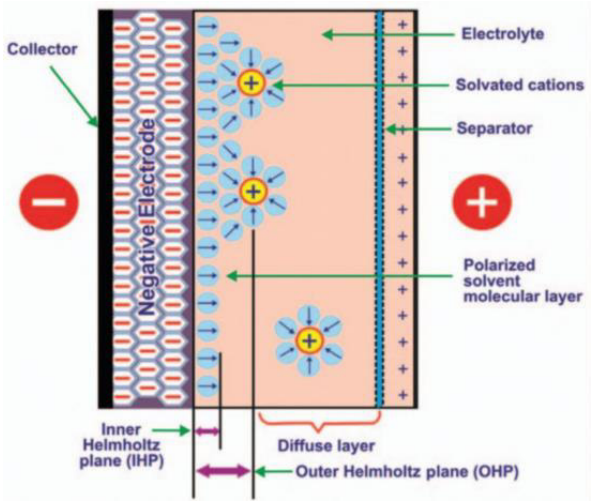

Figure 1.7 Voltage distribution across a charged EDLC and the equivalent electric circuit [69]

Both electrodes will contribute to C_1 and C_2 in load separation-related capacitance, as illustrated in Figure 1.7 when coupled in a series connection. There is a sensation of resistance here due to the existence of R_1 and R_2 collectors and the internal R_i resistance caused by the movement of ions inside the electrolyte. Using Figure 1.7, the capacitance behavior of the double layer may be described.

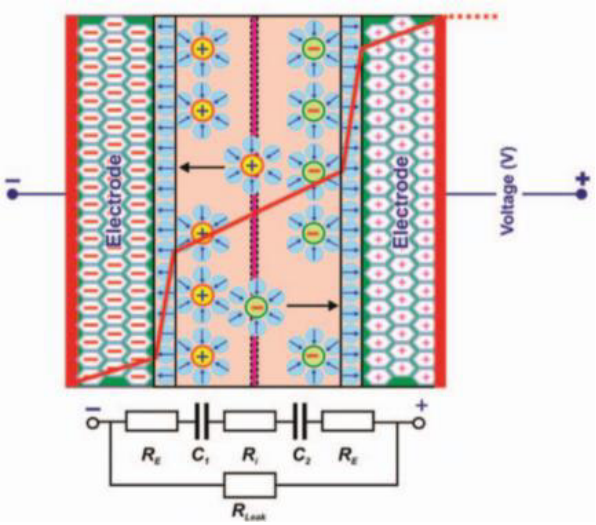

Figure 1.8 Model illustrating the double layer capacitance [69]

In this model, different forms of polar solvents, such as water, have been employed on organic liquids like methanol and acetonitrile. Because dipoles in solvent molecules interact with the charged electrode surface, they can move closer to the electrode surface with the oppositely charged end. Adsorbed electrolyte ions are explicitly present in this layer. Because the other components partially cover the electrode's surface, the ions are partially encased by the solvent molecules. The water molecules and the electrolyte-charged ions compete. Both molecules and ions prefer to be close to the layer connected with the electrode's surface. The IHP is a monolayer of solvent molecules with a thickness equal to one electrolyte molecule. Between the opposing changes, this creates a dielectric medium. The OHP extends from the electrolyte to the center of the dead ion, forming one double layer. With a change in distance, potential disparity arises along the Helmholtz plane. The potential fluctuation throughout the dual-layer and in the diffuse layer of the bulk solution is seen in Figure 1.8. The Stern layer, also known as the double layer, broadens to the OHP. As a result, the double-layer capacitance is made up of a series

connection between the Helmholtz plane/ Stern layer capacitance and the diffuse layer capacitance, as shown in Fig. 1.9.

$$\frac{1}{C} = \frac{1}{C_s} + \frac{1}{C_D} \qquad 1.13$$

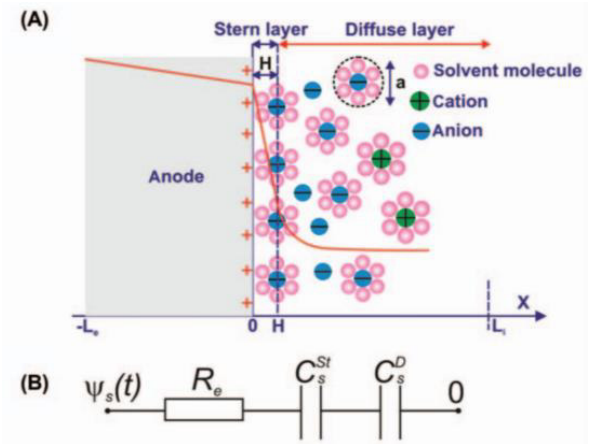

Figure 1.9 A. Process and, B. Electric circuit, describing the split in the capacitance between the stern layer and the diffuse layer [69]

The Stern layer capacitance is C_s, whereas the diffuse layer capacitance is C_p. As previously stated, the electrodes formed two parallel plate condensers, resulting in a single EDLC cell with two capacitors linked in series. To obtain the net capacitance in both electrodes, a series of capacitance must be applied. The corresponding circuit of an EDLC cell is shown differently in Figure 1.9. The resistance of the isolating layer, R, is believed to be adequate. Due to capacitance and resistance across the double layer, the circuit shows a parallel combination of C_{dl} and R_p. Until recently, the best carbon materials had double-layer capacities of around 150 Fg^{-1}, with the pore size of the carbon being adjusted using ionic liquid electrolytes. The energy densities of EDCL can be improved by surface functionalization with nitrogen and oxygen. Furthermore, if the pore diameters match the size of the electrolyte ion, redox-active electrolyte species can be used.

The creation of ionic liquid combinations, as well as the improvement of cell voltage and temperature range, can all help. The use of 2D graphene for EDLC is also becoming increasingly common. Due to the use of graphene, which has a large surface area, the specific capacity can be increased by up to 100-250 F. On the other hand, the gravimetries-normalized capacitance may be problematic due to graphene's nanoscale sheet-like morphological characteristic. Graphene may be used to construct the flexible device designs of EDLCs.

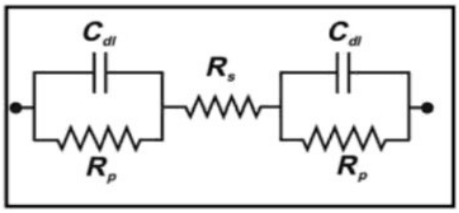

Figure 1.10 Equivalent electrical circuit of an EDCL cell

1.4.3 Pseudocapacitance [70-75]

The development of electrical double layers is the mechanism of pseudocapacitors. The insertion and adsorption of ions from the electrolyte into/on the electrode surface and reduction-oxidation reactions from the load storage start this process. Because the mechanism is almost two-dimensional, charging and discharge rates are comparable to EDLCs. Due to the presence of chemical processes, the system's capacity grows. A hybrid between a battery and a dual-layer capacitor is a pseudocapacitor. Due to the existence of an electrolyte between two electrodes, it is also formed. Chemical and electrostatic methods are used to store charge. During the reduction-oxidation (redox) reaction, the changeover on the electrolyte is part of the chemical process due to applying thinner redox compounds across the electrode's surface during charging. This is also owing to the fact that electrolyte ions have a reduced penetration rate. Multiple processes in

pseudocapacitors store charge, resulting in increased capacitance values. A cell containing a pseudocapacitor is shown in Fig. 1.9.

C is the potential-dependent pseudo-capacitance, as seen in the corresponding electrical circuit in Fig. 1.10. C may readily surpass the double-layer capacitance C_{dl} at specific potentials. RF is the electrode-electrolyte resistance, and RD is the faradaic resistance that can act when the ions desorb. The parallel arrangement of capacitors helps create the capacitance of pseudocapacitors due to the additive law of capacitance.

Pseudocapacity can be used to describe faradic energy storage. The reaction on the electrodes' surface or near-surface region is essentially based on a rapid redox reaction. Electro sorption/electro desorption happens during charging by moving charges across the electrode without substantial phase alteration. The charge status (q) is determined by the electrode's voltage and the amount of charge/discharge transmitted. The derivative values, dQ/dV, rise as Q values vary around potential.

Chapter 2. Methodology

2.1 Introduction

This chapter goes into great length on the study's methodological choices and research design procedure. It has mostly depended on the philosophical attitude and the research challenge to lead the methodological solution to improving energy storage. The literature review in the first chapter on supercapacitors features and development indicated the importance of combining studies on material and electrical properties of energy storage, particularly in the field of material design of electrodes, which provide the underlying principles of the research methodology for this thesis. These two fields have given the research both depth and breadth while also shaping the design of this research. This chapter aims to describe the data collection method of study and other related issues that were encountered during the material preparation process. In this chapter, three main sections contribute to the description of the research methodology. The first two sections represent the material preparation and the process we have used in our research; in the last section, information is given on data gathering and research procedures applied with a measurement tool.

It is also informative to state that our research has been divided into four parts, as mentioned in figure 2.1. The primary concern of this research is to find a way to improve the electrical properties of electrodes in supercapacitor structure, although other terms of energy storage have been explored. We used an experimental method to investigate our research goal and find a better algorithm. In this method, the research question has been defined in the first step as a guide for the next phase. As mentioned in the second step, we surveyed the last research work to determine a new theory for electrode material

fabrication. In the next step, our case study in different formats has been built, and various tests have been conducted to find how much improvement was made by a new theory. In the last step, we expanded our theory to other input parameters to generate a basic chain rule for energy storages electrode fabrication.

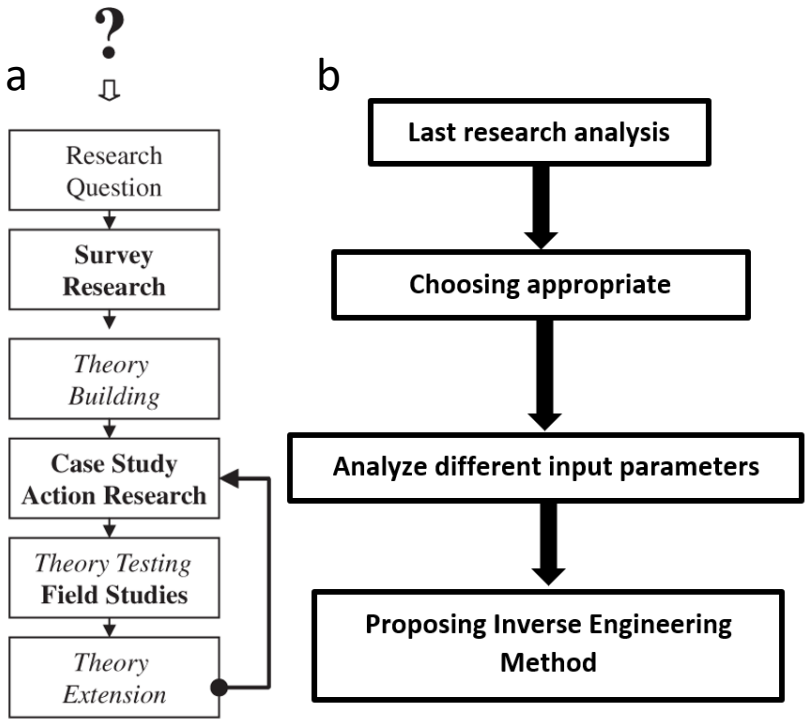

Fig 2.1 a) Proposed research structure, b) Applied research flowchart

2.2 Laser [76-79]

As mentioned in the last part, pulsed laser ablation has been used in our sample preparation as the most prominent feature of a pulsed laser; high power density and narrow frequency have been offered in different tests. However, it could be affected by wrong parameters selection. Pulsed operation of the lasers refers to any laser not classified as a continuous wave. In other words, we can call any laser with a specific frequency or duration of repetition a pulsed laser. Although this technology contains many applications, it could be

found in a simple laser that cannot generate continuous power. In some applications, pulses with high energy in the shortest time are needed; on the other hand, a gradual repetition of power impact should be seen. In the laser ablation, for example, a small volume of material at the surface of a workpiece can be evaporated if it is heated in a short time, whereas supplying the energy would allow for the heat to be absorbed into the bulk of the piece. In some applications, researchers rely on the peak pulse power instead of energy in pulse, especially when they are looking for non-linear optical effects. This requires creating pulses of the shortest possible duration for specific pulse energy utilizing techniques such as Q-switching.

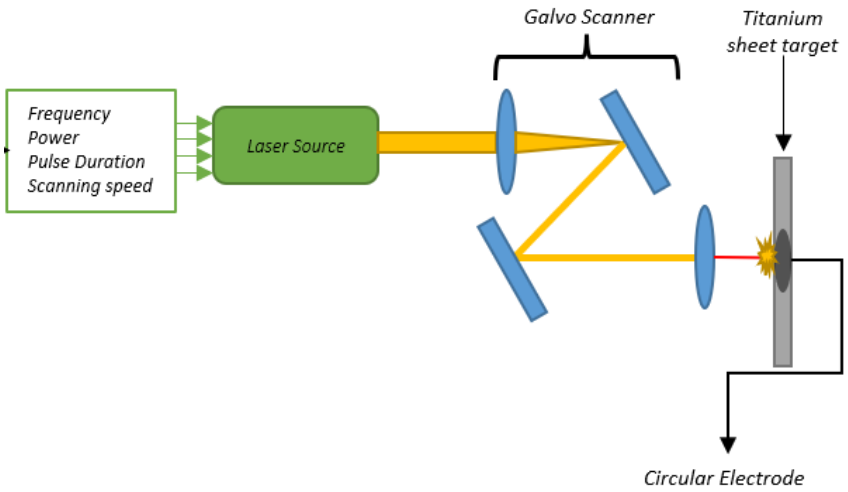

Figure 2.2. Electrode deposition by laser

Pulsed laser tools have been making a significant effort for commercialization in the last decade and are used in several applications, such as biomedical, electronic, and storages devices. Although the capital cost has been increased, the efficiency and improvement have been shown to be significantly better. The energy storage industry, like other fields, needs modern routes to emerge as a substation of different traditional generations. Improved energy storage system costs, service life, durability, and power density are made possible

by innovative materials that enable new storage technologies, such as a low-cost membrane or high capacitance supercapacitors. Although pumped-storage technology has more than %80 energy efficiency through a complete cycle, supercapacitors are emerging as the fastest and most reliable electrical storage.

Nanomaterials are currently used as one of the energy storages options. PLA as a high technology tool can help us modify our candidate material to see how much improvement will be seen. We benefited from a picosecond Ytterbium pulsed laser (IPG Germany) employed as a beam source. This high peak power laser emits clean, ultrafast pulses centered at 1035 nm (Detailed specifications, including typical pulse intensity and power scaling with repetition rate, are available [22]). The pulsed laser ablation method has been used in our research. A physical laser ablation technique with a high-power pulsed laser beam is focused on our material (Titanium) to generate TiO_2. This material is vaporized from the target (same material as substrate) and deposited on the surface. It has been shown in figure 2.2 that thin TiO_2 sheets were produced by Ytterbium pulsed fiber laser (IPG Laser Model; YLPP-1-150V-30) with a 1064 nm wavelength. The laser diameter of 7.6 mm was reduced to 6 mm using an *iris* diaphragm which was then focused toward an XY galvanometer scanner (JD2208 by Sino-Galvo). Also, we employed an appropriate F-theta lens with a focal length of 63.5 mm, an input aperture of 14 mm, and a beam displacement of 18.7 mm. The scanner provided a theoretical laser spot diameter of 20 µm. The interfacing software used to set patterning parameters was Marking Mate 2.7 in Kiani's lab where equipped with a pulsed laser setup illustrated in figure 2.2.

After the laser ablation process, we had to choose one of our options to make the best shape for electrodes depending on the project phase. Our project includes two main phases; where

the first one was run with NRC (National Research of Canada), and the second phase was conducted entirely in Kiani's group, which will be described in the following parts.

2.3 Potentiostat [80]

In this part, we review a basic overview of the working principle of potentiostat/galvanostat. Depending on the application, this machine can be used differently to make different information about electrical or corrosion properties. As we show in figure 2.3 internal circuit of the potentiostat contains some electronic devices for figuring properties of materials. Each properties test needs a specific potentiostat configuration, although we can substitute them in some cases. In electrochemical spectroscopy, we look for electrical features of materials that need to find voltage, current, electrical resistance, etc. Conductivity, capacitance, rate of charge, and discharge are a sample of parameters we chose to analyze with this machine. A potentiostat/galvanostat (PGSTAT) in potentiostatic mode will precisely control the potential of the counter electrode (CE) against the Working Electrode (WE) so that the potential difference between the WE and the Reference Electrode (RE) is well defined. It corresponds to the value specified by the user. Calculating this difference allows us to determine how much the voltage can be modified in energy storage under various scenarios. The CE is linked to the output of an electrical block called a Control Amplifier (CA), as shown in figure 2.3. Current is forced through the cell by the control amplifier. For low and high currents, a Current Follower (LowCF) or a Shunt (HighCR) is used to monitor the current value. With a Differential Amplifier, the potential difference between RE and S is continuously observed (Diffamp). The PSTAT/GSTAT switch is adjusted according to the mode of the instrument (potentiostatic or galvanostatic). The signal is then supplied into the Summation

Point (Σ), which will be utilized as an input for the control amplifier and the waveform established by the digital-to-analog converter (E_{in}).

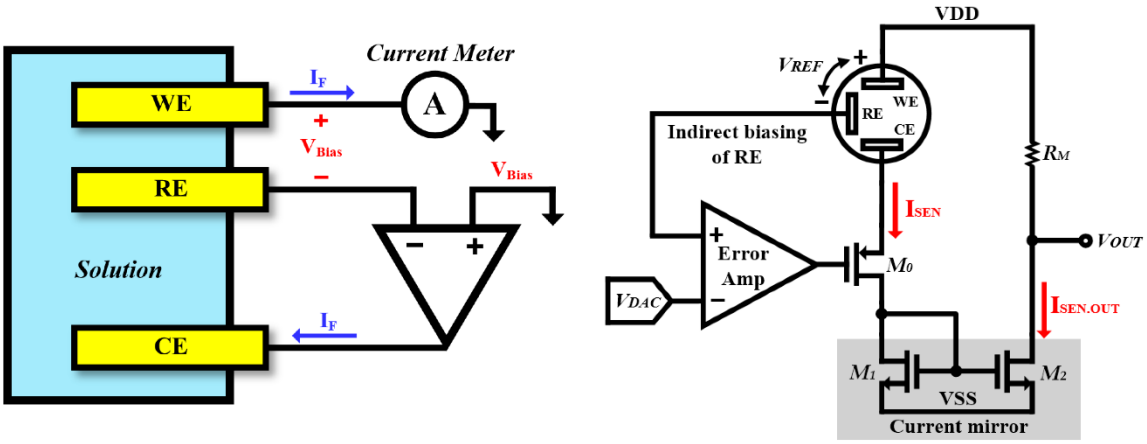

Figure 2.3 Internal circuit of potentiostat [81]

The electrodes that have been used in our experiments include a wide range of frequency, power, pulse duration, and scanning speed in the fabrication process; then, we used a standard configuration for electrochemical tests. The counter electrode (also known as an auxiliary electrode) is an electrode that is used to close the current circuit in the electrochemical cell.

It is generally made of an inert substance (such as Pt, Au, graphite, or glassy carbon) and doesn't become involved in the electrochemical reaction. Because of the current flows between the WE and the CE, the CE's total surface area (source/sink of electrons) must be greater than the WE's to ensure that the kinetics of the electrochemical process under research is not blocked. The reference electrode is an electrode in the electrochemical cell with a stable and well-known electrode potential. It is utilized as a point of reference for potential control and measurement. A redox system with consistent (buffered or saturated) concentrations of each redox reaction participant is frequently used to achieve great

stability of the reference electrode potential. Furthermore, the current flow across the reference electrode is kept near zero (preferably zero) by utilizing the CE to close the current circuit in the cell and a very high input impedance on the electrometer.

We used a potentiostat machine in two phases, including symmetric and asymmetric supercapacitor structure, which is based on the reference and working electrode. In symmetric structure, potentiostat has two similar functions for two ports and cannot be assigned any electrode to the positive or negative side. In asymmetric design, positive and negative electrodes can be specified up to the charge/discharge process.

Generally, potentiostat can be used in two, three, and four-electrode setups for different applications, although we only used two electrode configurations. The three-electrode cell setup is used in electrochemistry more than other setups, which is defined the current flows between the CE and the WE parts in experimental setup. The potential difference is controlled between the WE and the CE and measured between the RE (kept at the proximity of the WE) and S. Because the WE are connected with S, and WE are held at pseudo-ground (fixed stable potential), by controlling the polarization of the CE, the potential difference between RE and WE are controlled all the time. The potential between WE and CE usually is not measured. This is the voltage applied by the control amplifier, and the compliance voltage of the instrument limits it. It is adjusted so that the potential difference between the WE and RE will equal the potential difference specified by the user. This configuration allows the potential across the electrochemical interface at the WE to control RE. The four-electrode setup is used for applications where the potential difference (between RE and S) occurs because the passage of a current across a well-defined interface (between WE and CE) needs to be measured. Usually, it is used to measure junction

potentials between two non-miscible phases or across a membrane, help to make it possible to calculate the resistance of the interface or the membrane conductivity.

2.4 Image Characterization

2.4.1 Scanning electron microscopy (SEM)

The first scanning electron microscope (SEM) debuted in 1938 [82] (Manfred von Ardenne), and the first commercial equipment appeared around 1965 [83]. However, the delay in development was due to the electronic parts that scanned the electron beam on the sample. An electron microscope is a scientific instrument that uses a beam of high-energy electrons to inspect an object on an excellent scale. The electron microscope was developed due to the limitations of the light microscope, which is limited by the physics of light in nature. In 1930, the theoretical limit was reached, and there was a scientific desire to see the details of the internal structure of organic cells (nuclei, mitochondria). This process required magnifications of more than 10,000, which was not possible with current light microscopy. SEM is an electron microscope that images a sample in a raster pattern by scanning a high-energy electron beam. The electrons interact with the atoms that make up the sample to create a signal that contains information about the sample's surface, topography, composition, and other properties. SEM shows four main properties of the material.

- Topography: The surface features of an object or its appearance, its texture.
- Morphology: The particle size and form that make up the object. There is a direct link between these structures and their material characteristics.

- Composition: The elements and compounds that make up an object and their relative quantities. The direct relationship between composition and material properties
- Crystallography: How atoms are arranged within an object and the direct relationship between these arrangements and material properties.

The main difference between Optical Microscope (OM) and an Electron Microscope (EM) is light sourcing. In OM, the light source is actual light, whereas, in EM, the light source is replaced by a beam of very fast-moving electrons. The specimen in EM usually has to be specially prepared and held inside a vacuum chamber from which the air has been pumped out because of less traveling of electrons in the air. In addition, the lens is replaced by a series of coil-shaped electromagnets through which the electron beam travels. The image has formed a photograph (called an electron micrograph) or on a screen.

The SEM images have a broad depth of field, allowing a significant portion of the sample to be in focus at once and producing an image that accurately represents the three-dimensional sample. SEM is one of the most widely used tools in academic lab research and industry due to its combination of higher magnification, bigger depth of field, better resolution, and compositional and crystallographic information. We chose SEM for the material survey because of all of SEM's capabilities and benefits in surfave properties analysis. In other word, SEM can help us to observe surfave structure before and after laser ablation.

We employed Hitachi's FlexSEM 1000 SEM at Ontario Tech University, which allows for improved imaging of specimen surfaces at high and low accelerating voltages with up to 5nm resolution. This machine is equipped with a Peltier-cooled energy dispersive X-ray

detector (EDS) for quantitative elemental analysis and mapping and the ability to operate in secondary, backscattered, and mixed modes.

For taking SEM images, firstly, we cleaned the specimen's surface in preparation for capturing SEM photographs. Because the surface of the sample can contain a variety of unwanted deposits, such as dust, silt, detritus, media components, or other contaminants, that may have happened before SEM specimen preparation, proper cleaning of the sample surface is required. The specimen was then treated using fixatives in the following stage. Fixation can be accomplished using different fixatives such as aldehydes, osmium tetroxide, tannic acid, or thiocarbohydrazide and perfusion and micro-injection immersions, or vapors. After the fixation step, samples were rinsed to remove the excess fixative. Other preparation steps of SEM configuration, such as rising the specimen, dehydrating the specimen, drying the specimen, mounting the specimen, and coating the specimen, were completed before running the image collecting.

2.4.2 X-ray Diffraction (XRD) [84, 85]

Another form of X-ray crystallography is X-ray Diffraction, in which a beam of X-rays strikes a sample (crystalline solid), lands on a piece of film, or lands on other detectors to create dispersed beams. To put it another way, XRD uses X-dual ray's wave/particle nature to gain information on the structure of crystalline materials. Experiments are carried out in XRD, as in other X-ray Crystallography, to determine the atomic and molecular structure. A beam of incoming X-rays diffracts into many different directions due to the crystalline structure.

The X-ray beams first create a diffraction pattern of spots recorded as the sample rotates, followed by the angles and intensities of the scattered beams, allowing a crystallographer to create a three-dimensional representation of the density of electrons within the crystal. In the next step, this electron density generated in the last step can help show the mean positions of the atoms in the crystal as well as their chemical bonds, disorder, and information.

XRD measurements were carried out for crystalline analysis with a Rigaku MiniFlex 600 diffractometer (Bragg-Brentano geometry) equipped with a NaI scintillation counter detector and a monochromatized Cu Kα radiation source (λ = 1.5406 Å) operating at a voltage of 40 kV and current of 15 mA. In an X-ray diffraction experiment, a sample is placed into the center of an instrument and illuminated with a beam of X-rays. The X-ray tube and detector move in a synchronized motion, then the signal is coming from the sample and is recorded, and graphed peaks related to the atomic structure of samples. As we know, most materials are made up of many small crystals like sand. Each of these crystals is composed of a nucleus surrounded by a cloud of electrons which created the first idea of XRD. X-rays as high-energy light with a repeating period called wavelength generate initial energy for showing the figures. Since the wavelength of an X-ray is similar to the distance between atoms in a crystal, a special interference effect or diffraction can be used to measure the distance between the atoms. In this step, the interference can be generated when X-rays interact. If the waves are in alignment, then the signal is amplified (constructive interference), or if the waves are out of alignment, the signal is destroyed (destructive interference). When an X-ray encounters an atom, its energy is absorbed by the electrons, which occupy special energy st ates around an atom.

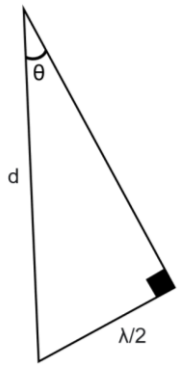

Figure 2.4. X-Ray diffraction beam [86]

Since this is not enough energy for the electron to be released, the energy must be re-emitted in the form of a new X-ray (Elastic Scattering). In a crystal, the repeating arrangement of atoms forms distinct planes separated by well-defined distances. When the atomic planes are exposed to an X-ray beam, they are scattered by the spaced atoms. Robust amplification of the emitted signal occurs at precise angles where the scattered waves constructively interfere (diffraction). The angle between the incident and the scattered beam is called 2Θ (Figure 2.4). In order for constructive interference to occur, the scattered waves must be in alignment, which means the second wave must travel a whole number of wavelengths. In this case, one-half of the wavelengths are crossed on the incident side and another half on the scattered side, yielding one additional wavelength. In the case of the subsequent X-ray, one wavelength has traveled on both the incident and the scattered side resulting in two wavelengths.

The triangle (Figure 2.4) determines the exact angle at which diffraction occurs. The angle at the top is Θ which is half of the angle between the incident and scattered beams. The long side is the distance between the atomic planes, and the short side we know as one-half of a wavelength. The relationship between the diffraction angle and the spacing between the atoms can be determined by applying the sin function (Bragg's Law)

$$sin\theta = \frac{\lambda}{2d}\ n\lambda = 2dsin\theta \qquad 2.1$$

X-ray diffraction helps scientists develop the new structure of materials in different fields that are the key to discovering new applications. As well as other applications, We believed XRD could help us determine the crystallographic structure of TiO_2. The benefits of this survey can affect the fabrication process of energy storage where we compare different surface structures to use them in supercapacitor.

2.5 Electrochemical Characterization [87-88]

Electrochemical characterization is a set of methods or techniques that uses electrical stimulation to survey the electrical behavior of material from their chemical reaction on the solution's surface. Oxidation and reduction reaction rates are controlled and measured by a potentiostat (electrochemical test machine). Electrochemistry is a branch of chemistry that relates to the interaction of electrical and chemical phenomena. Electrochemists deal with the study of chemical changes when electric current moves in the material when a chemical reaction happens. The name electrochemistry comes from the oxidation-reduction reaction. Generally, electrochemical methods contain classified ways to measure the potential, charge, or current to determine the electrical character of chemical reactivity. Electrochemists utilize qualitative and quantitative analysis methods based on electrochemical processes that occur inside a medium or at the phase border and are connected to changes in the structure, chemical composition, or concentration of the molecule under investigation. Methods of electrochemistry may be classified into five categories.

Potentiometry: finding the concentration of a solute in solution. The potential between two electrodes is measured using a high impedance voltmeter in potentiometric measurements.

Voltammetry: the combination of voltage (in n electrode structure when dipped into a solution) with amperometry. A varying potential is applied to a working electrode in an electrochemical system in voltammetry, and the corresponding current is measured.

Coulometry: is an electrochemical method in which the total charge (the number of coulombs) consumed in the redox conversion of analysis at an electrode is measured.

Conductometry: is about studying the electrolytic conductivity of the reacting species or resultant products. This analysis is based on the fact that during the charge/discharge, one ion is replaced by the other, and invariably, these two ions differ in ionic conductivity.

Di-electrometry: the field of measuring permittivity of a solution as a function of concentration.

In addition to basic analysis in electrochemistry, we can use some specific experiments to see how different materials can behave in other conditions. We selected cyclic voltammetry, electrochemical impedance spectroscopy, and charge/discharge methods to show how our proposed material can improve supercapacitor structure efficiently.

2.5.1 Cyclic voltammetry

Cyclic voltammetry (CV) is the most frequently used technique that scientists are using to study electrochemical reactions and provide information on the reversibility and kinetics of chemical reactions. In CV, the electrode's potential is repeatedly scanned linearly from an initial potential to a final potential. The potential in which the maximum current occurs

is known as the peak potential (E_p), where the redux time has been finished on the electrode surface and the current diffusion limited. The magnitude of the Faradaic current (anodic or cathodic) indicates the rate at which electrons are being transferred. CV graph can be reversible, quasi-reversible, and irreversible.

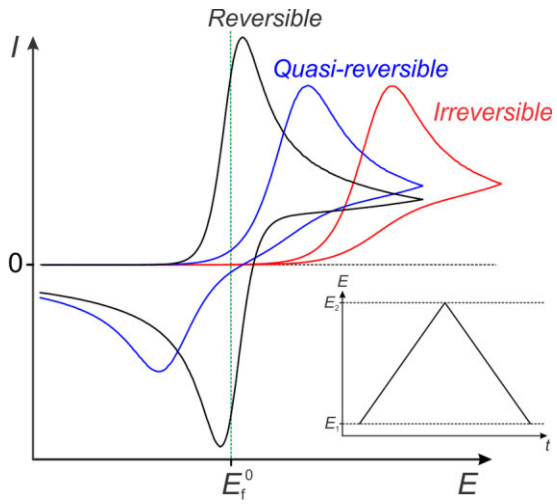

Figure 2.5 Typical Cyclic Voltammetry graph for the reversible process [90]

Reversible Process: a chemical process in which the whole system can be returned to the initial state from the final condition without changing properties. Specifically, in electrochemistry, the electron transfer process is rapid and equal in oxidation and reduction in a reversible process.

Irreversible Process: defined as the chemical process with finite time for completion in one direction. In this type of reaction, equilibrium may exist only after completing the process. In the charge/discharge process, only the forward oxidation (reduction) peak is observed.

Quasi-Reversible Process: this process is controlled by both the mass transfer regime and the kinetics of the electrode reaction. This process happens when the relative electron

transfer rate of mass transport is inadequate to maintain Nernst equilibrium at the electrode surface. CV test is a kind of adaptable electrochemical technique assigned to probe the mechanics of redox and transport properties of the system in solution. The working electrode potential is ramped linearly versus time to make a CV graph. In the CV test, we can use all electrode structures; when the active electrode reaches a set potential, the ramp is inverted. This inversion might occur numerous times (one cycle cannot be helpful for analytical tests). The cyclic voltammogram trace is created by plotting the current at the working electrode vs. the applied voltage throughout these cycles. The potential is applied between the reference electrode and the working electrode, and the current is measured between the working electrode and the counter electrode. As all CV graphs show, the potential direction should be reversed at the end of the first scan to form an isosceles triangle (Figure 2.6).

As shown in Figure 2.6, the reduction process runs from (a) initial potential to (d) switching potential. In this area, the potential is negatively scanned for reduction. The resulting current is called the cathode current (i_{pc}). The corresponding peak potential occurs at (c) called the cathode peak potential (E_{pc}). When all the substrate is reduced on the surface of the electrode, it reaches the E_{pc}. After getting the switching potential (d), the potential scans positively from (d) to (g). This causes anodic current (I_{pa}) and oxidation. The peak potential of (f) is called the anode peak potential (E_{pa}) and is reached when all the substrates on the electrode surface are oxidized. Since our tests are based on a reversible process, some equations are useful for this type of structure. The electron potential is the sum of the potential changes of the initial potential (switching point) (E_t) and the time interval (vt).

$$E = E_{t,s} \pm vt \qquad 2.2$$

Electron stoichiometry (n), where:

$$E_p - E_{\frac{p}{2}} > \frac{0.0565}{n} \qquad 2.3$$

E_p is the cathodic peak potential, and n is the number of electrons participating in the redox reactions. Formal reduction potential ($E^{\circ\prime}$) is the mean of the $E_{pc}$and E_{pa}values:

$$E^{\circ\prime} = \frac{E_{pc} + E_{pa}}{2} \qquad 2.4$$

Cyclic voltammetry can be used to study qualitative information about electrochemical processes under a variety of conditions.

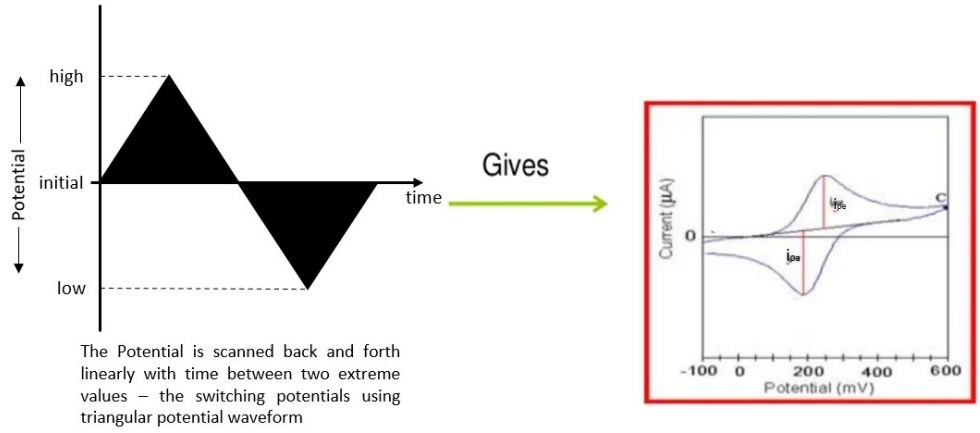

2.6 Cyclic Voltammetry Basic Principles [91]

2.5.2 Electrochemical Impedance Spectroscopy

Electrochemical impedance spectroscopy (EIS) specializes in various electrochemical methods. Classic electrochemical techniques provide measurements of current, charge, or electrode potential as a function of time (which may also be related to electrode potential). In contrast, EIS presents a signal as a function of frequency at a constant potential. This often causes problems in understanding what is happening, as electrochemical try to think

in time rather than frequency. On the other hand, no one believes that light consists of sinusoidal vibrations of electrical and magnetic vectors of different frequencies, phases, and amplitudes in optical spectroscopy. In spectroscopy, we considered the frequency domain (wavelength, frequency, or related function as wavelength) and observed the Fourier transform of the optical signal. There are many benefits to using EIS. First, it provides a lot of helpful information that can be further analyzed. Practical applications of cyclic voltammetry measure simple information about peak currents and potentials. These parameters contain little information about the entire process, especially if the hardware and software can sample the current-potential curve and generate thousands of experimental points with any mV function. Few people in the current study, on the other hand, know and use this technique, but they can use convolutional voltammetry, which provides all possible information. The EIS contains valuable information about all frequencies where we can compare the function of electrical storage in different applications. In this study, we use EIS to analyze the impedance behavior of supercapacitors to compare how laser ablation can improve the surface's ability to absorb ions in the charge/discharge process.

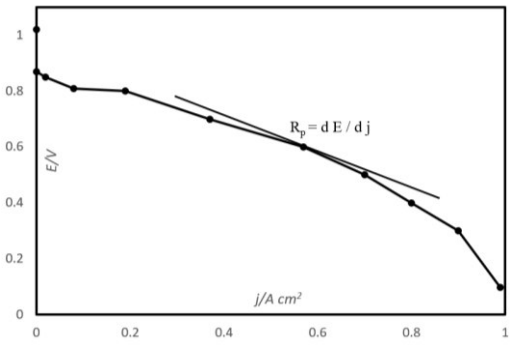

2.7 Impedance spectroscopy basic principles

A steady polarization measurement, that is, a measurement of current at a constant potential, provides a current-potential curve from which the gradient, i.e., polarization resistance $R_p = \frac{dE}{dj}$ can be determined. Figure 2.7 shows an example of such a curve for a fuel cell.

However, acquiring impedance at each potential produces a series of data values at different frequencies. Figure 2.8 shows complex plane impedance diagrams of different fuel cells' imaginary and real parts at different frequencies. The graph shows that the polarization resistance is the only point corresponding to the zero frequency. It turns out that the impedance curve provides much more information than R_p, which is not available in steady-state measurements. The impedance diagram shows a complex curve that is rich in information. Such information is included at every point, not just the value of R_p. However, we need to know how to find this information about the system under investigation. This is a more complex problem and can be solved by proper physicochemical modeling. Figure 2.7 shows an example of a fuel cell complex plane impedance diagram. Polarization resistance was also seen in steady-state measurements. Further study must be carried out and fully understood before EIS analysis to characterize a more complex electrochemical system. This includes microscopic, surface morphology, structure, composition, and DC electrochemical characterization.

EIS uses circuit analysis tools developed in electrical engineering. The mathematical foundation of EIS was laid by Heaviside, who developed the calculus and Laplace transform of operations and introduced the differential (S) and integral (1/S) operators. They made it possible to solve the integrodifferential equations that appear in the solutions of electrical circuits by transforming them into a system of algebraic equations. Heaviside

explained the relationship between the Laplace transform and the Fourier transform by defining impedance, admittance, reactance, and operating impedance and introducing the complex operator $s = \sigma + j\omega$. The main advantage of EIS is that it is based on the linear time-invariant system theory, commonly known as LTI system theory, and the validity of the data can be confirmed by the integral transform (Kramers Kronig transform) that does not depend on the related physical process.

To understand the impedance of an electrochemical object, we need to understand the behavior of a simple electrical circuit, first in the steady-state and then in the transient state. Such circuits include simple linear electrical elements such as resistors, capacitances, and inductances. EIS results require an understanding of the Laplace and Fourier transforms. To understand impedance, you need a complete understanding of the complex plane and the Bode plot (we use both analyses in our study). They can be calculated with special programs like Excel, Maple, Mathematica, and ZView; however, we used EC Lab software for our experiments

Nyquist Plots: At this point, it is helpful to explain the most common methods for displaying EIS spectra and extract useful information from them. The first is the Complex Impedance Plane. In this plot, the data from each frequency point is plotted by the imaginary part on the vertical axis and the real part on the horizontal axis. Representing Z_{Im} (also known as Z, or Z_j,) on the y-axis so that the data fits in the first quadrant of the graph is a common rule in electrochemistry. This type of diagram helps identify the number of distinctive features the system has, but all frequency information is lost. To recoup this, the frequencies of important data points such as high and low intercept and the

characteristic frequencies of the arc should always be annotated. This characteristic frequency is the frequency at which the Z_{Im} is maximized.

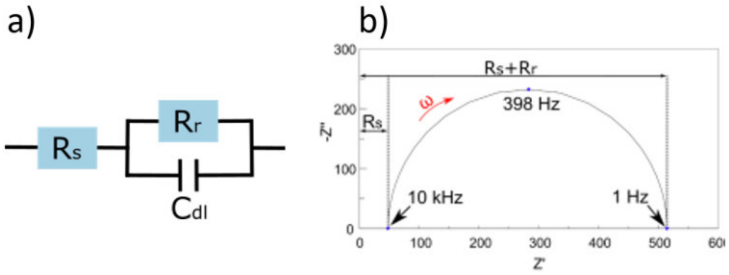

Figure 2.8 a) Circuit model used in EIS tests, b) Nyquist plot in EIS [92]

Figure 2.8 b shows an example of the Nyquist diagram where the circuit in figure 2.8 (a) has values $R_s = 47$, $R_r = 467\Omega$, and $C_{dl} = 860nF$.

Bode Plots: impedance values and phase angles are plotted against frequency in the Bode plot. The magnitude and phase angle are in equations 2.5 and 2.6, respectively.

$$|Z| = \sqrt{Z_{Re}^2 + Z_{Im}^2} \qquad 2.5$$

$$\varphi = tan^{-1}\left(\frac{Z_{lm}}{Z_{Re}}\right) \qquad 2.6$$

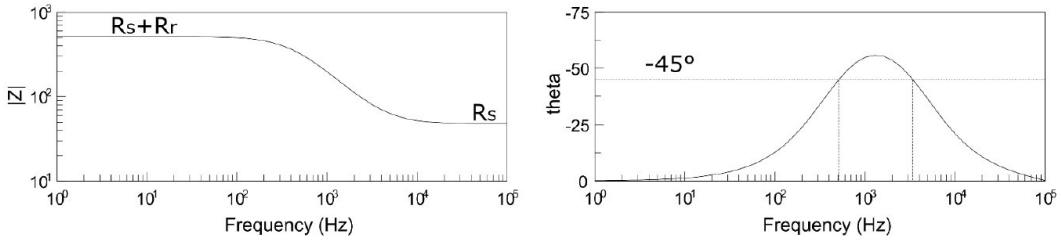

Figure 2.9 Bode plot in EIS [92]

Because the large range of values frequently encountered in | Z | is represented on a logarithmic scale, small values are easy to find. The high-frequency limit of | Z | also applies, yielding R_s, while the low-frequency limit yields $R_s + R_r$. The degree of the

imaginary part's frequency dependence is indicated by the rate of change in the transition zone between the two asymptotic limits. The frequency at which -45° = 0 should be the feature's characteristic frequency. On the other hand, this example touches this line at both f = 500Hz, and f = 3,300Hz. This inaccuracy is caused by R's high-frequency dominance, which obscures the behavior of the process that is responsible for the EIS function. As a result, the R_s estimate should be deducted from the 4.444 real and imaginary components of the whole dataset. As a last remark on EIS, region-specific impedance data is commonly acquired by multiplying the real and imaginary components of the impedance by the electrode's cross-sectional area.

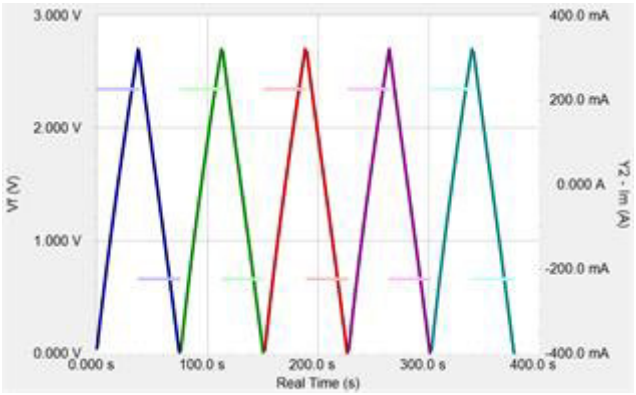

Figure 2.10 Charge/discharge diagram [92]

2.5.3 Charge/discharge

The Cyclic Charge Discharge (CCD) method is a widely used method for evaluating the performance and longevity of EDLC and batteries. A cycle is when the charging and discharging loop is repeated. Charging and discharging are normally carried out at a steady current until the desired voltage is obtained. Each cycle's charge (capacity) is monitored, and the capacity C in farad (F) units is determined using the formula C = Q/V. The charge in Coulombs is Q, and the voltage window is V. Both are graphed as a cycle count function. The capacitance curve is the name given to this curve. Charges are more usually referred

to as capacity in practice. Normally, capacity is measured in amp-hours (Ah), with 1 Ah equaling 3600 coulombs. The actual number of cycles reveals the capacitor's usable life when the capacitance reduces by the given value (usually 10% or 20%). Commercially available capacitors can go through hundreds of thousands of cycles. Figure 2.11 shows the CCD data recorded with the 3 FED LC model. Five cycles are plotted against time with current and voltage, and each cycle is graphically represented in a different color. The bright waveform is the current being supplied to the capacitor. The darker-colored waveform shows the measured voltage. The capacitor was cycled between 0 V and 2.7 V with a current of ±0.225 A.

This new EDLC has nearly optimal behavior: the curve's slope (dV/dt) is constant and is determined by Eq. 2.7:

$$\frac{dv}{dt} = \frac{I}{C} \qquad 2.7$$

Where V is the potential of cell in volts (V), I is the current of cell in amperes (A), and Q is the charge in coulombs (C) or amperes seconds (A.s). Figure 2.11 shows the same CCD process with a 3F capacitor damaged by overvoltage. The behavior of this capacitor is clearly far from ideal.

The charge and discharge voltages vs. time take exponentially shape as self-discharge increases. A higher equivalent series resistance (ESR) results in a significant voltage drop (IR-drop) at each half-cycle, drastically reducing power and capacity. As a result of the charge/discharge loss, the EDLC's efficiency has been drastically diminished.

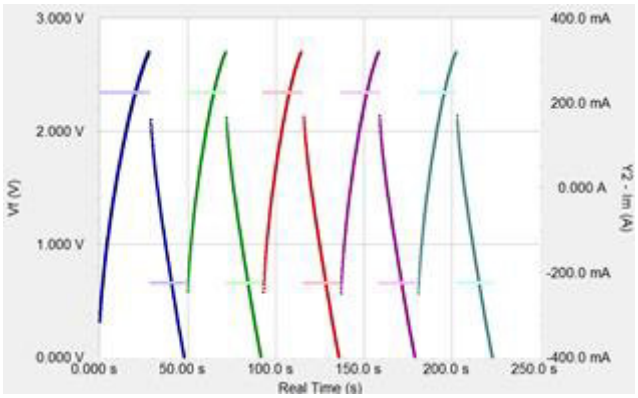

Figure 2.11 cyclic Charge/discharge diagram [92]

2.5.4 Lifetime

Cycling is a standard experiment for evaluating a battery's long-term stability. The capacity of batteries is assessed after they have been charged and discharged hundreds of times.

A standard cycle charge-discharge (CCD) experiment for batteries is shown in Figure 2.12. The coin cell was first charged at a rate of 1.0 C to 4.2 V. (40 mA). After that, the potential was potential-statically maintained for at least 72 hours or until the current reached 1 mA. After that, the battery was discharged at a rate of 1.0 C to 2.7 V. For 100 cycles, this procedure was repeated. The darker curves show the capacity. The lighter curves represent the percentage of capacity compared to the start.

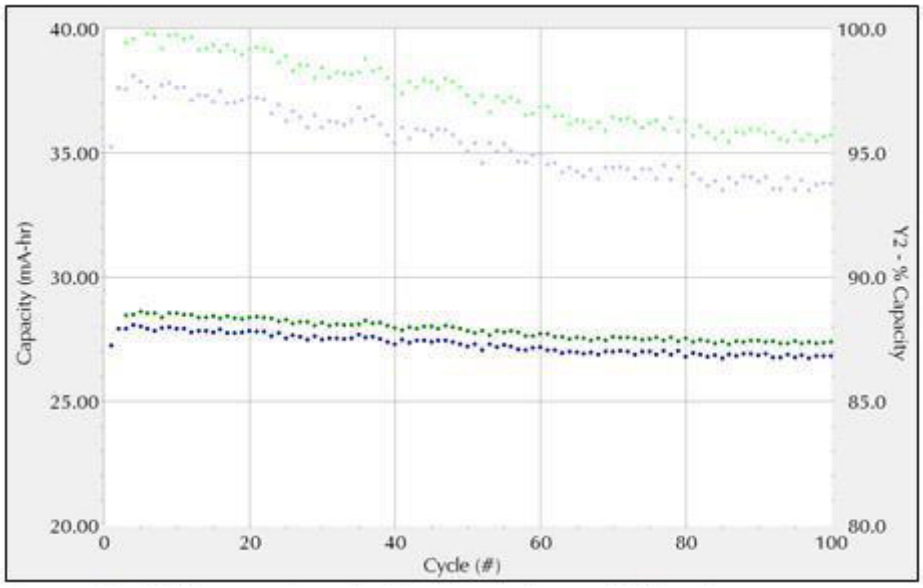

Figure 2.12 CCD experiment of a coin cell over 100 cycles [92]

Impurities in the electrolyte or imperfect electrodes invariably result in capacity loss. In this case, the tested battery has a decent cycling behavior. This battery's maximum capacity is approximately 28.7 mAh. After 100 cycles, capacity just marginally declines. The overall capacity loss is around 4.5%.

Extreme temperatures, as well as overcharging or discharging, can hasten capacity degradation. When a battery's capacity is lost by more than 20%, it's time to replace it.

The Echem Analyst also allows you to calculate the Coulombic efficiency. This term describes the charge ratio when discharging and charging (see equation 2.8).

$$\eta_C = \frac{Q_{discharge}}{Q_{charge}} 100\% \qquad 2.8$$

Chapter 3. Laser Parameters [93-95]

3.1 Introduction

Electrochemical features such as charging/discharging mechanism and life cycles in gas sensors, lithium-ion batteries, and other types of electrical storage are only a few applications for porous-structured thin films. The porous structure thin film has a specified surface area and can allow for a very short ion diffusion path. Controlling the surface morphology of TiO_2 thin films has piqued interest as a means of developing materials. The shape of TiO_2 thin films allows for a wide range of applications. Chemical bath deposition, sol-gel procedure, anodic electrochemical deposition, hydrothermal method, thermal decomposition, and pulse laser ablation method are some of the physical and chemical techniques used to make the TiO_2 thin film. The electrochemical properties of the TiO_2 thin film are improved by uniform shape, film thickness, purity, and adjustable pore size.

A pulsed laser ablation is an approach for fabricating high-quality thin films useful for fine-tuning their properties. There are, however, a few studies on the synthesis of TiO_2 thin film arrays utilizing PLA. On the other hand, there has been a lot of research into pure Titanium Oxidation at high and low temperatures. Cathodic precipitation and sol-gel dip coating are the two most used procedures for obtaining TiO_2 thin films. We also used a combination of PLA and coating to make Titanium thin films in this investigation.

Titanium dioxide (TiO_2) has been shown to be an effective material for photocatalysis, dye-sensitized solar cells, heterogeneous catalysis, self-cleaning/antifogging surface coatings, and other applications. TiO_2 is commonly used in two forms: powder and thin film. Crystalline TiO_2 powder is commonly used for gas and liquid phase catalysis. Particle size,

phase composition, and the position of the conduction and valance bands on the energy scale are all factors that influence its photocatalytic activity. TiO_2 is commonly employed in photovoltaic applications such as photoelectrochemical systems (PEC) and dye-sensitized solar cells (DSSC) for photon harvesting in thin-film form. Furthermore, by potentially biassing the photoanodes, TiO_2 in thin-film form offers the advantage of energy alignment between the valance band edge's energy location and the electrolyte's redox species. This aids in optimizing quantum efficiency.

Metalorganic chemical vapor deposition (MOCVD), sol-gel, electrophoretic deposition, reactive rf sputtering, and pulsed laser ablation are some techniques used to manufacture TiO_2 thin films. PLA is a high-energy method that produces a highly adherent thin film with strong mechanical stiffness and surfaces with a high specific surface area. Furthermore, PLA has advantages such as stoichiometrically moving material from the target to the substrate, inert and reactive gas deposition capacity, a wide range of operational pressure and temperature, and a choice of substrate material possibilities.

As has been shown previously, no research groups have investigated TiO_2 thin films produced by pulsed laser ablation. However, different types of the method were used to fabricate electrodes in supercapacitor applications. Several groups observed anatase and rutile multiphase formations in TiO_2 thin films. Only Luca et al. [96] have studied the relationship between anatase phase composition and oxygen partial pressure. However, no potential mechanism was proposed. The PLA approach differs from chemical-based synthesis (e.g., Sol-Gel and MOCVD) in that multi-valance Ti species are typically produced during the deposition process. This is unusual in chemical synthesis methods due to oxygen molecules in the precursor itself. It is generally operated in an oxygen-rich

environment. Based on optical measurements of the laser ablation plume, Kitazawa [97] discovered the presence of neutral and ionized Ti and TiO species even with a TiO_2 target. The reduced TiO_2 surface (oxygen vacancy) is particularly interesting for photocatalysis applications such as formic acid dehydration and water molecular dissociation. Few research has looked at the link between Ti valence states and deposition conditions during the PLA synthesis of TiO_x thin films. According to Luca et al. [96], the O: Ti ratio ranges from 1.78 to 2.0 at various temperature and pressure combinations. The ratio = 4 also found that when the deposition was performed at 423K, TiO_2 and its suboxides (i.e., TiO and Ti_2O_3) coexisted.

The pulsed laser ablation of TiO_2 is straightforward, yet it involves a complex physical phenomenon. Variations in ablation parameters like pressure and temperature result in various chemical and structural compositions. Only a few papers on thin films made by PLA techniques have investigated the films' photocatalytic capabilities. To avoid the production of amorphous TiO_2, Dr. Kiani's group produced TiO_2 thin films using the PLA method at substrate temperatures of 873 and 1073 K in this study [77]. Pressures ranging from 250 to 750 mTorr of buffer gas (O2: Ar =1:1) were utilized to prevent the development of suboxide TiO or Ti_2O_3. We slightly reduced stoichiometric TiO_2 films with a consequent fluctuation in the rutile/anatase phase composition by operating the PLA system within these temperature and pressure ranges. A conductive substrate is necessary for solar applications. The quartz substrate was covered with indium doped tin oxide (ITO), one of the most extensively used transparent conductive oxides (TCO). This work describes the surface topography, crystalline structure, Ti binding energy, quantum efficiency

spectra, and photocurrent onset of TiO_2/ITO thin films generated under various temperature and pressure synthesis circumstances.

3.2 Preparation of TiO_2

The pulsed laser ablation of TiO_2 is simple, but it involves a complex physical phenomenon. Variations in ablation parameters such as pressure and temperature result in various chemical and structural compositions. Only a few reports on pure TiO_2 thin films prepared by PLA methods have tested the film's photocatalytic activities.

[93] has already described the experimental setup. We simply provide the key parameters of the ablation technique. With a fluence of 3 J/cm', the beam of a KrF excimer laser (A = 248 nm) was focused on the revolving target. A halogen light heated the substrate to a temperature of 790°C. The deposition chamber had a base pressure of 4 X 10d8 mbar, although the film was ablated at a pressure of 10:l mbar. The films were cooled at a pressure of 200 bar of oxygen. The targets were made from TiO, rutile powder with very fine grains (about 10 nm), compressed and sintered in air at 1050°C up to 56% of the bulk density while maintaining the rutile structure determined by X-ray diffraction and Raman spectroscopy. MgO (1001, Si coated with a SiO, amorphous layer about 1 pm thick, and AlO, films were produced on well cleaned monocrystalline substrates: MgO (1001, Si covered with a SiO, amorphous layer about 1 pm thick, and AlO. The focus of the discussion will be on these examples in particular. TiO is found in three distinct crystalline phases: anatase, rutile (tetragonal), and brookite (orthorhombic). When heated, amorphous TiO crystallizes into anatase, which changes into rutile above roughly 700°C. Depending on the deposition processes and settings, amorphous TiO (at low substrate temperatures in general), anatase and rutile phases, or both, with varying proportions, orientations, and

crystal sizes, can be obtained. We employed X-ray diffraction and SEM to characterize the structure.

The effect of quadruple laser parameters on the electrochemical and physical properties of electrodes will be discussed in this section. We will look at the potentiostat data in the electrochemical survey to understand how fabrication parameters affect the electrical behavior of electrodes in the supercapacitor. We will explain how different laser parameters can create diverse porosity structures in addition to electrical behavior.

3.3 Laser Parameters Analyze

In this section, we will discuss the effect of four laser parameters on the electrochemical properties of the supercapacitor. We used the coin cell platform to compare electrochemical properties in all tests.

3.3.1 Deposition Cycle

The main factor we have been considering in the preparation of TiO_2 electrodes is the porous value on the surface of the active side, which directly relates to electrochemical properties. PLA generates a high-power pulsed laser beam focusing on the material surface and generating holes to increase the ability to absorb ions in energy storage function. We assumed with the doubling of laser ablation of the material surface, the porosity would be increased. With this assumption, we repeated the laser ablation process with the same parameters one time to see how it affected the physical and electrochemical properties of electrodes. Figure 3.1 shows how a laser beam can generate porous on the surface. As we can see, repeating the laser process or remelting the porous area will increase r (radius of the hole), which means the electrode can place more ions in the charging process. Although the center of circles in the proposed double laser process are not necessarily the same, we

have a non-uniform structure in the porous material. This non-uniform structure can be considered between the ideal double deposited and single deposited holes. In addition to the positive aspect of doubling the electrode deposition, the negative points should also be considered. As an example, excessive increment of laser power can lead to the destruction of electrode structure (we have noticed this phenomenon with the black material surface).

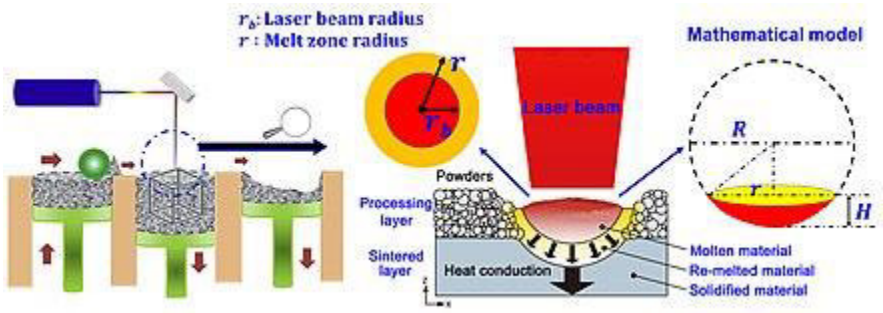

Figure 3.1. Laser beam deposition process [78]

In doubling the laser ablation on the electrode surface, we should consider different factors to get an optimum result (best hole structure). Other laser parameters, rest time between first and second deposition, and period of ablation (which relate to scanning rate) can affect the shape of the hole on the surface and, consequently, change the electrode's electrochemical properties.

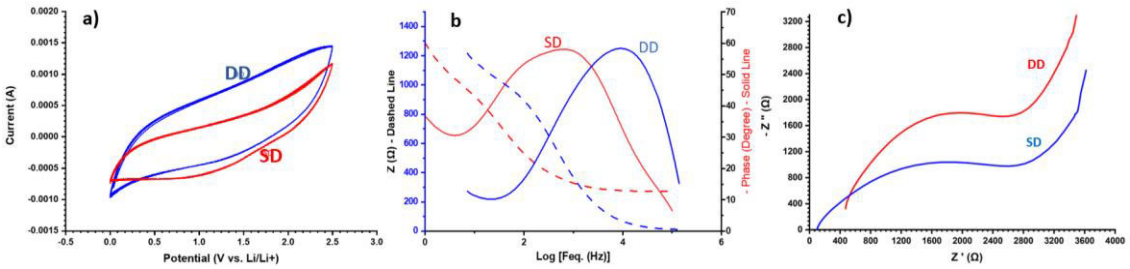

Figure 3.2 (a) cyclic voltammetry, (b) bode, (c) Nyquist

We tried to make ablation on the surface with equal laser parameters after a reasonable rest time (about five minutes between first and second deposition). We compared the

electrochemical properties of the electrode when it was deposited one time and two times to further investigation. As we can see in figure 3.2(a) area of the CV graph was increased when we deposited the electrode for the second time. Increasing the CV area means the energy storage capacity has increased by increasing the surface's hole size. This phenomenon can be justified as follows: size and shape of the hole as the location for ion absorption in electrical energy storage can be improved by increasing the amount of r. the blue line shows a double ablated electrode in the CV graph where we have better current in the charge-discharge process. The specific capacity of the double ablated electrode is 62 mF/g which is more than C_{sp}=51 mF/g in the single ablated. Bode figures for both single deposition and dual deposition have been shown in figure 3.1(b). When we compare these two samples, behavior in high-frequency, DD shows the best phase and magnitude. In f =10000 Hz phase is 1200 and 500, respectively, which means double deposition is more capable of saving energy. This superiority is shown in the Nyquist graph, where a double deposited electrode has lower resistance than a single deposition.

Considering all cases, it can be said increasing the number of depositions improves the electrochemical behavior of electrodes by increasing the size of porosity on the surface.

3.3.2 Frequency

As it was mentioned in the last part, the laser we used in the fabrication process can generate different frequency values. We applied different frequency values when we used PLA in the fabrication process. These various frequency-generated electrodes have been published in [79]. FEI Quanta 3D 200/600 scanning electron microscopy was used to examine the surface morphology of the samples (SEM, Hillsboro, OR, USA). The chemical compositions of the laser-irradiated materials were determined using a Rigaku Ultima IV

X-ray diffractometer (XRD, Austin, TX, USA) and Raman spectroscopy (Renishaw Raman Imaging Microscope System 2000, Renishaw, Mississauga, ON, Canada).

The topology of the electrode surface was altered by altering the laser frequency from 600 to 1200 kHz, as seen in SEM pictures in Figure 3.3. In general, laser-induced porous structures on the electrode surface with a large surface area may absorb more ions during the charge and discharge process; as a result, a larger surface area (increased porosity) can result in superior capacitance behaviors [98, 99]. The number of nanofibrous structures and porosity reduces as the frequency rises from 600 to 1200 kHz (Figure 3.1 a–c).

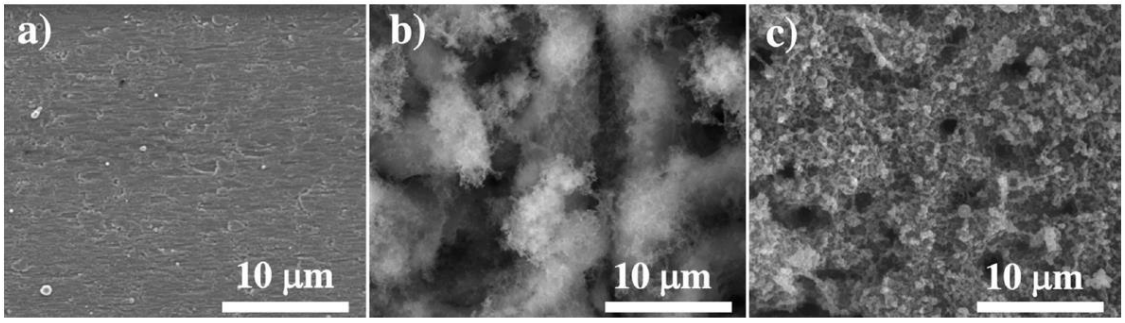

Figure 3.3 SEM image of electrode surface a) no deposition b) deposition with f = 600kHz c) deposition with f=1200 kHz [94]

Figure 3.1 depicts samples 2 (S2) and 3 (S3) microstructure. We can prepare at 600 kHz (T2) (S2: 69 m and S3: 43 m). ImageJ (v. 1.501 by Wayne Rasband at the National Institutes of Health, USA) assessed the porosities of S2 and S3 to be 59 percent and %36, respectively, with a %5 margin of error. Surface porosity is assumed to be applied to the volume of active materials, resulting in density values of 1.85 g/cm3 and 2.44 g/cm3 for electrodes treated at 600 and 1200 kHz, respectively. The active material mass for electrodes manufactured at 600 and 1200 kHz may thus be determined to be 10.02 and 8.24 mg, respectively.

The amount of oxidation that happened during the laser irradiation process is another difference between S2 and S3, which can be seen in the micro-Raman data shown in Figure 3.4 b. Figure 3.4 (a) shows that the anatase phase at 144 cm and the rutile phase at 443 and 610 cm have sharper peaks, indicating a larger presence of Ti oxide in S2.

As we mentioned in our paper [95], for the control sample, there are only two main peaks of Ti (101), and Ti (110) observed. For the samples with T3DN, the observed diffraction peaks were indexed to Ti(101), R(111), A(200), R(220), and Ti (110) in accordance with titania anatase (JCPDS card No.21-1272) and titania rutile (JCPDS card No.88-1175). It has already been proven in [93] that the peaks of rutile and anatase are sharper in the sample with a higher amount of T3DN (S2).

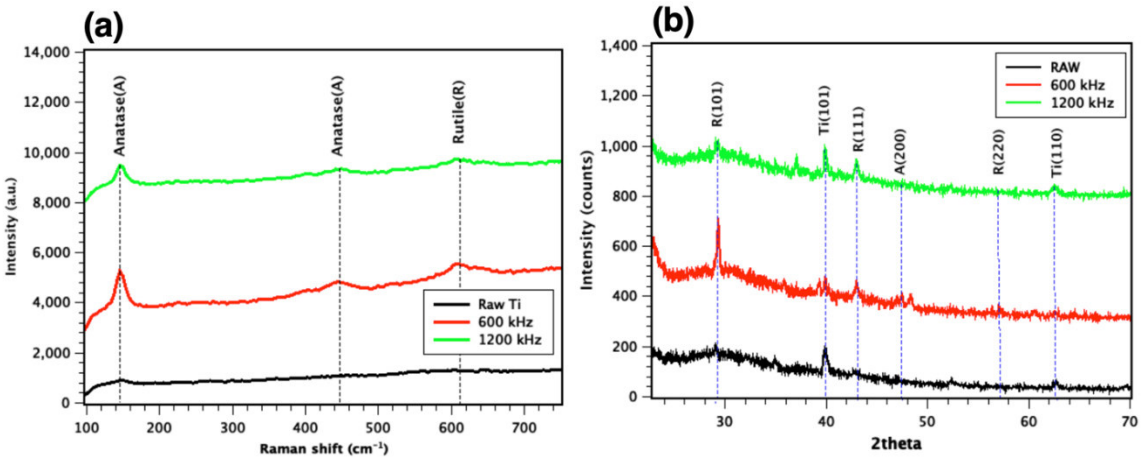

Figure 3.4. physical properties of S1, S2, S3 (a) Raman and (b) XRD [94]

In comparison to the Ti sheets treated at 1200 kHz, the SEM, Raman, and XRD data show that S2 has fewer fibrous features and greater oxidization rates (S3).

Because each pulse contains more energy, the maximum surface temperature of the irradiated zone is higher at the lower frequency of 600 kHz, resulting in a faster oxidation rate. The laser-plasma plume is more stable at a higher frequency of 1200 kHz, resulting

in a more significant aggregation of ionized atoms and evaporated nanoparticles, resulting in thicker nanofibrous formations.

Theoretical Models for Surface Temperature:

A theoretical model [100] was adapted to estimate the surface temperature of the Ti sheets at various pulse frequencies to study the influence of laser frequency on the plasma plume temperature (Figure 3.5).

The 3D radial temperature gradient is derived from our unique theoretical model.

$$\Delta T(r,z,\tau) = \frac{I_{max}\gamma\sqrt{k}}{\sqrt{\pi}K}\int_0^{\tau}\frac{p(\tau-t)}{\sqrt{t}\left[1+\frac{8kt}{W^2}\right]}e^{-\left[\frac{z^2}{4kt}+\frac{r^2}{4kt+0.5W^2}\right]}dt \qquad 3.1$$

The radius of the laser spot and the depth of the laser heat-affected zone, respectively, are r and z, and K is titanium thermal conductivity. The peak intensity is I_{max}, γ is 1-R (R is the Fresnel reflectance), and W is the (1/e) field radius. For square-shaped pulses at the ablation center, $p(t)$ is also equal to 1.

As seen above, the average and maximum surface temperatures are reduced when the laser pulses' frequency is increased. Theoretical and practical results concur as we predict an increased oxidation rate in S2 processed at 600 kHz compared to S3 processed at 1200 kHz at higher temperatures. In reality, the frequency of the laser has an effect on both the surface area (porosity and nanofiber formation) and the degrees of oxidation. The electrochemical characteristics of supercapacitors are influenced by these two parameters, which will be discussed in the next section.

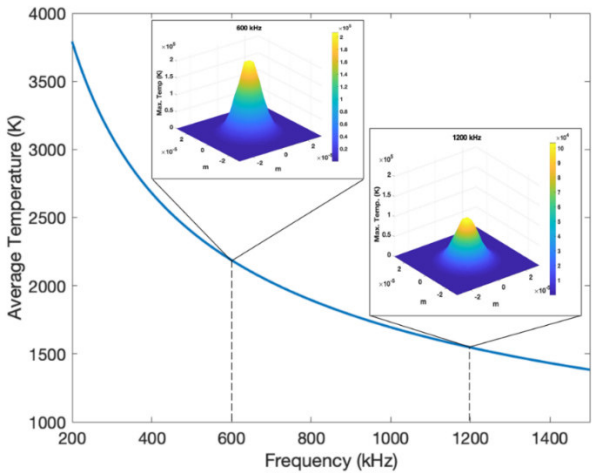

Figure 3.5. Temperature model of PLA in different frequencies [94]

The electrochemical characteristics of various applications such as energy storage and supercapacitor manufacturing were evaluated using the cyclic voltammetry technique, which can offer a large quantity of information quickly. From 200 mV/s to 500 mV/s, the CV curves of T3DN electrodes in 1M LiPF6 in EC: DEC exhibit a roughly rectangular shape, showing adequate capacitive behavior (Figure 4.4a). The type of electrolyte has an impact on electrochemical performance. We didn't focus on this issue because it was the same for all testing. The data given in Figure 4.4 suggest an overall improvement in S2 compared to S3. We determined that the laser frequency influence on topology and oxidation levels is responsible for this improvement. Based on a comparison of supercapacitor CV curves, a lower laser frequency can result in a larger thickness in electrode manufacturing. Figure 4.4 shows that the integrated area for S2 is much bigger than the areas computed by OriginPro in CV plots for T3 and T1. The following formula may be used to calculate the specific capacitance of the specified supercapacitors [101]:

$$C_{sp} = \frac{A}{2(V_2 - V_1)\left(\frac{\Delta V}{\Delta t}\right)m} \qquad 4.2$$

where A represents the area under the curve (AV), $\frac{\Delta V}{\Delta t}$ represents the scan rate (V/s), m represents the electrode weight, and V_1 and V_2 (V) represent the applied voltages in the experiments. At 500 mV/s, the specific capacitances of S2 and S3 are determined to be 59.85 and 54.39 mF/g, respectively. Table 3.I contains the parameters for additional scan rates. C_{sp} for S2 and S3 may also be determined using the following formula:

$$S = 2(V_2 - V_1) \times m \times C_{sp} \qquad 4.3$$

S is the slope of the fitting line in the "area vs. scan rate" plot (see Figure 3.4b). As a result, the C_{sp} values for S2 and S3 are 43.6 and 39.2 mF/g, respectively.

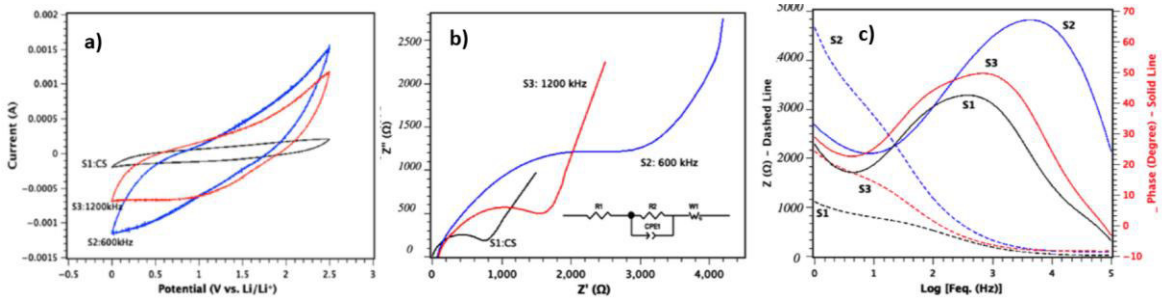

Figure 3.6. (a) cyclic voltammetry, (b) bode, (c) Nyquist [94]

Table 3.I Additional scanning rate of cyclic coltametry test

Sample	Scan Rate (V/s)	Potential Window (V)	Mass of Active Material (g)	Area (AV)	C_{sp} (F/g)
S2	0.500	2.5	0.01002	0.0014826	0.05918563
	0.400			0.001469	0.07330339
	0.300			0.001442	0.09594145
	0.200			0.0012018	0.11994012
	0.020			0.0004284	0.42754491
S3	0.500	2.5	0.00824	0.001120548	0.05439553
	0.400			0.001050816	0.06376311
	0.300			0.000954892	0.07644757
	0.200			0.00089702	0.09551214
	0.020			0.000312004	0.37864563

Figure 4.4c shows the findings for C_{sp} at various scan speeds ranging from 20 to 500 mV/s. The results demonstrate that as the scan rate is increased from 20 to 500 mV/s, the specific capacitance drops, which might be attributed to a variety of factors such as pore-size distribution, and the existence of both micro-and mesopores and specific surface area, as previously reported. At lower scan speeds, charged nanofibrous structures have more time to interact with other fibers and holes of T3DN electrodes in both S2 and S3.

The CV findings show that the greater quantity of T3DN and higher oxidation rate in S2 enhances C_{sp} retention, favoring higher power density, as shown in Figure 3.4c, with the maximum value for C_{sp} for S2 being 427.5 mF/g at 20 mV/s. Indeed, the greater T3DN production aids electron transit during the charge-discharge process.

This shows that by varying laser parameters (pulse frequencies) that directly affect 3D-Nanonetwork fabrication and oxidation levels in the generated active material surface, it is possible to customize the capacitive behavior of T3DN electrodes, demonstrating that it is possible to customize the capacitive behavior of T3DN electrodes.

The number of leaps (to Q = 0.032 C/cm^2) in three samples may be seen in charge/discharge, which is represented in Figure 4.5. As indicated in the experimental setup, we employed two separate electrodes for all three supercapacitor types, implying we may have comparable but somewhat different behavior on both sides (electrodes in each setup). If we call the specific capacitance of negative and positive electrodes $C_{negative}$ and $C_{positive}$, we get the following equation:

$$C_{abs} = \left|C_{Positive} - C_{Negative}\right| \qquad 4.4$$

The absolute difference in electrode capacitance is referred to as Cabs. We discovered that increasing the number of Cabs leads to a larger number of leaps by comparing three charge/discharge graphs. The jump values above relate to the electrode's saturation time and can be utilized as qualitative data to describe the behavior of energy storage devices [102]. For example, in the first 50 cycles of S2 and S3, there are 16 and 21 leaps, respectively; in S1 (control sample), there are only four jumps due to electrode capacity saturation. In comparison to S2 and S3, the S1 supercapacitor takes less time to get saturated during charge and discharge cycles and has the lowest capacitance [103]. When it comes to electrode capacitance and saturation time, S2 outperforms the other two electrodes (S1 and S3)

$$(C_{positive,I} = n_{S1} \times C_{negative,I}, C_{positive,II} = n_{S2} \times C_{negative,II}, C_{positive,III} = n_{S3} \times C_{negative,III}) \rightarrow n_{S3} > n_{S2} > n_{S1} \quad 4.5$$

Figure 4.6a shows the Nyquist plot of electrochemical impedance spectroscopy measurements for bare titanium (S1: Control Sample) and T3DN electrodes (S2 and S3) across a frequency range of 1 Hz to 100 kHz. According to the data, all three samples displayed a semicircle in the high-frequency range. Higher oxidation levels in electrodes (S2) manufactured at a pulse frequency of 600 kHz resulted in a higher radius for the semicircle areas, which may be ascribed to the barrier to electron transport inside the electrode materials higher oxidation levels in electrodes (S2). Electronic and ionic contributions determine the supercapacitor's overall impedance [104]. The inherent barrier to electron transport and the interfacial resistance of the particles govern the electronic contribution. The ionic contribution is determined by ion diffusion resistance toward pores and electrolyte resistance within pores [105].

S2 has a vertical line in the low-frequency area compared to S1 and S3, owing to greater ion transport in the electrolyte to the electrode interface, resulting in higher performance of T3DN electrodes manufactured at 600 kHz (S2).

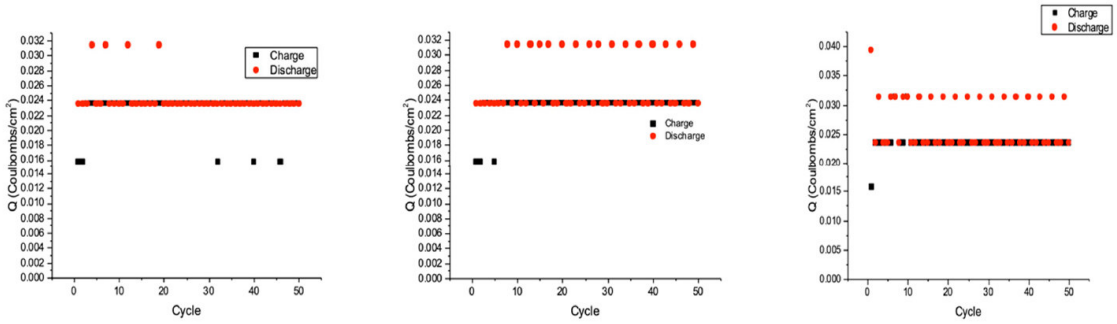

Figure 3.7. Charge/discharge graph of samples [94]

The overall impedance reduces with increasing frequency in low-frequency zones, as indicated in the Bode plot in Figure 4.6b. On the other hand, the frequency-independent diffusion resistance is connected to the impedance area, which is observed at a higher frequency. In [79] electrolyte ions into the electrodes in most cases, at high frequencies, when compared to the control sample, the capacitance behavior of the S2 and S3 electrodes is greater (S1). Furthermore, in the Bode plot, S2 has the highest phase angle of 67°, which is closer to the phase angle of an ideal capacitor (90°) than S3 (48°) or S1 (41°). At a phase angle of 45°, the capacitor response frequency (f0) could be measured, and the relaxation time constant ($t_0=1/f_0$) was determined to be 0.25 ms and 1.56 ms for T2 and T3, respectively.

A serial connected R1, R2||CPE2, and W1 were developed according to the equivalent circuit model used in this research (Figure 6a). The Ti sheet (substrate) is represented by R1, and the T3DN layer is represented by R2||CP2. Constant phase element (CPE) is a characteristic that may be used to assess if a circuit element is acting like a capacitor or a

resistor, according to earlier research [106, 107]. CPE is a factor connected to the Nyquist plot's depressed semicircle, which is termed Q or CPE-T and CPE-P. The values of CPE-P range from 0 to 1 (zero for the ideal resistor and 1 for the ideal capacitor), while CPE-T corresponds to the amplitude. In summary, in a supercapacitor, a lower R2 and CPE-T value, as well as a CPE-P value closer to 1, are preferred. Figure 4.7 shows that for S2, CPE-P has the closest value (0.76) to 1 and CPE-T has the lowest value compared to S3 and S1.

Figure 4.7 also shows that S2 has the lowest resistivity (R2) compared to the other samples. Compared to S3 and S1 (which have the lowest performance), S2 has the greatest outcomes for CPE-T, CPE-P, and R2; the differences are due to the larger quantity of generated T3DN in S2 as well as its higher oxidation level. As previously stated, the temperature of the fabrication process is higher at 600 kHz, resulting in the formation of a thicker layer of T3DN with higher porosity on the electrode sheets. In general, electrodes with a larger surface area and more oxidized Ti have a greater surface area and ion diffusion. Fabrication factors like frequency, pulse duration, intensity, and the number of pulses may be used to adjust the topology and oxidation levels of the created T3DN in the proposed approach. In this study, we primarily focus on the influence of frequency, but other factors for the manufacture of optimum advanced electrodes will be examined in the future direction of this research.

The influence of pulse frequency as a critical manufacturing parameter on the electrochemical performance of T3DN electrodes was studied in this part. To analyze the produced nanostructures' morphology and their compositions, we changed the pulse frequency from 600 to 1200 kHz and performed morphological and material

characterization studies. We discovered that lowering the pulse frequency allows for the formation of more nanofibrous structures with greater oxidation rates. Theoretical methods for calculating the average and maximum surface temperature confirmed this fact.

The higher surface area and oxidation rate of electrodes generated at 600 kHz result in better electrochemical performances, as demonstrated by CV, charge/discharge, and EIS analyses. Samples fabricated at 600 and 1200 kHz had specific capacitances of 59.85 and 54.39 mF/g at 500 mV/s, respectively. The performance of the T3DN-based supercapacitors may be modified for different applications by adjusting the pulse frequency. By offering new methodologies for EES and supercapacitor production, we are certain that this pulse ionization technology will open new doors to this developing and fast-growing sector. Our suggested approach is a one-step, environmentally friendly procedure because no chemicals are employed in the fabrication process, and it can be carried out under normal settings. In addition, the T3DN may grow directly on Ti sheets without the need for any binder or conducting active agent material, which decreases fabrication time and cost while also reducing resistance between the current collector (Ti) and active materials. Other laser parameters (e.g., pulse duration, pulse power, pulse number) will be examined in the future as part of this research to discover the optimal parameters for fabricating enhanced supercapacitor electrodes with predefined electrochemical characteristics.

3.3.3 Power

In this part, we will show how the power of laser ablation can affect the electrochemical properties of supercapacitors. Laser power controls the amount of energy absorbed into the working sheet. In general, the bend angle increases with laser power attains a peak and

decreases with different laser power. At a higher power laser beam, the material is heated to generate a larger volume of porosity, which means more energy storage, as we said in the last part. Although mentioning this critical point will be helpful that increasing the power more than the threshold amount can damage the electrode surface, which means we should calculate the power amount which results in the best electrochemical properties.

As we mentioned in equation 4.2 specific capacitance of electrodes can be calculated when we have the area of the CV graph. Same as last part, we tried different parameters for laser power, and we concluded better electrochemical properties had been seen when we increased the amount of power in the fabrication process. As it is seen in table 4.II, when we increase the power, the specific capacitance of the supercapacitor has been increased. Other electrochemical properties of supercapacitors show better behavior when power increases in the fabrication process. Charge/discharge retention (lifetime of supercapacitor in long term use) is %73 when we use 15 w for generating both electrodes, although it is %83 in the last case scenario (Power = 20 w)

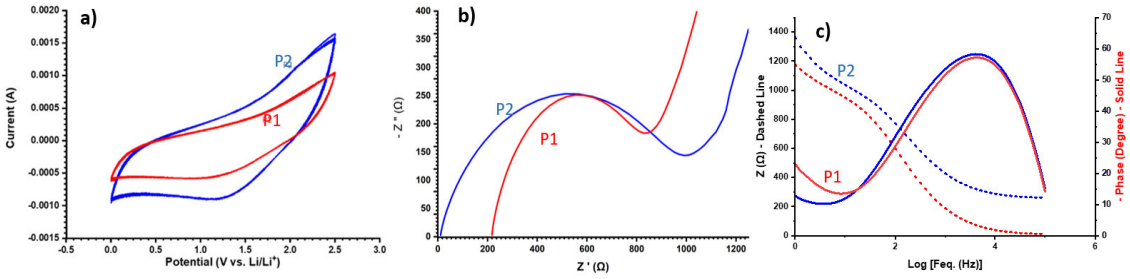

Figure 3.8 (a) cyclic voltammetry, (b) bode, (c) Nyquist

3.3.4 Pulse Duration

Pulse duration is one of the laser parameters which we used in the material fabrication process. The period of the laser beam is the time from the start of one pulse to the next. The pulse duration (pulse width) is the time measured across a pulse, often at its Full With

Half Maximum (FWHM). The pulse duration depends on several parameters: the type of gain medium and how much energy it can store, the cavity length, the repetition rate of the pulses, and the pump energy, to mention the most important ones. Q-switched lasers commonly used in the industry can produce average powers up to tens or hundreds of watts and repetition rates as low as 10 Hz or as high as 200 kHz. Most industrial processes are in the kilohertz to tens-of-kilohertz regime.

The actual Q-switch device is an acoustic-optical modulator or an electro-optical modulator (EOM). Both use crystals where an applied electric field produces some perturbation of the crystal's optical properties. In the case of acoustic-optical modulators, the applied electric field is a radio-frequency voltage that produces a high-frequency sound wave in the crystal. This sound wave diffracts the photons from the laser and prevents laser amplification. EOMs use an applied high voltage that modifies the crystal refractive index and alters the polarization of the incoming light; an appropriate combination of polarization-sensitive optics can be placed in the cavity to prevent light of altered polarization from circulating.

Other types of lasers, such as excimer lasers, do not require a Q-switch to produce nanosecond pulses but rather rely on a transient pump pulse: Excimer laser pulses are produced by exciting the noble gas/halogen mixture with a powerful and short electric discharge. Ti: sapphire lasers can also produce nanosecond pulses if they are pumped with a nanosecond pulse of green light produced by a frequency-doubled, Q-switched YAG laser. This method is called gain switching because the cavity gains rather than the can make the same amount of phase and different amounts of magnitude in electrodes.

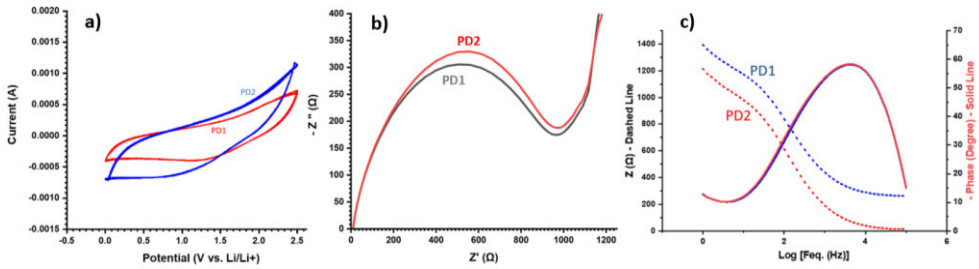

Figure 3.9. (a) cyclic voltammetry, (b) bode, (c) Nyquist

Apart from a huge number of industrial applications, Q-switched lasers have important applications in scientific research. One is pumping of Ti: sapphire ultrafast amplifiers (described in the following section) by using the frequency-doubled (green) output of a Q-switched Nd:YAG or Nd:YLF at 1-10 kHz. Another one is using the YAG or YLF laser to produce energies per pulse in the joule range at 1-100 Hz. These lasers are often used with nonlinear optical generators that can produce tunable wavelengths in the UV, visible and IR region, enabling time- and wavelength-resolved studies. Nowadays, most YAG or YLF lasers operating at >100 Hz are diode-pumped, while high-energy 10-Hz systems require pumping with a flashlamp because diodes are not suitable for producing high-energy output pulses. For some scientific applications, it may be desirable to have a narrow-linewidth Q-switched laser. In some cases, this can be accomplished using a combination of optical gratings and etalons; in other cases, the laser can be “seeded” with a low-power CW or Q-switched narrow-linewidth laser that is easier to control than the higher-power stage. This approach, called “injection seeding,” uses a MOPA (master oscillator, power amplifier), conceptually splitting the linewidth selection and the high-power generation into two optimally designed stages for the two purposes.

Cavity loss is directly changed.

As we can see in figure 3.9, PD1 results in lower specific capacitance and current in the cyclic voltammetry test. This behavior could be the result of that PD1 generating smaller porous on the surface, which leads to a smaller capability of energy saving. Impedance behavior in pulse duration analysis can be another factor that helps us to decide about this parameter in the fabrication process. PD2 shows higher capacitance in the Nyquist plot, where we can say this sample can lead to better behavior in storage applications. Although the Nyquist graph shows PD1 and PD2 can generate the same behavior for phase, the difference in impedance magnitude is the result of different capacitance. In other words, we can mention the different amounts of pulse duration

Chapter 4. Optimization

4.1 Introduction

A common sort of challenge in machine learning and artificial intelligence is classification [108, 109]. This chapter covers and contrasts four popular categorization techniques: logistic regression, support vector machine (SVM), and single hidden layer neural networks. A classification problem's purpose is to predict the value of a variable with discrete values. The purpose of binary classification is to predict a variable that has only two possible values, such as determining a person's gender (male or female). The purpose of multi-class classification is to forecast a variable with three or more possible values, such as predicting a person's state of residence (Alabama, Alaska, Wyoming). A regression problem is one in which the goal is to forecast a numerical value, such as a person's annual salary. There are dozens of Machine Learning (ML) classification techniques, and most of them have many variants. One method for conceptualizing ML classification techniques is to categorize them into three groups: math equation classification techniques, distance and probability classification techniques, and tree classification techniques. This chapter will go through three of the most frequent math equation categorization methods to offer an appropriate method for energy storage fabrication purposes. Because so many different areas utilize categorization, each concept has multiple names. Predictor variables, for example, are also known as features (in data science), signals (in electrical engineering), characteristics (in social sciences), and independent variables (mathematics). The variable to be predicted is also known as the class, label, or dependent variable. In our project, we tried to use three different ML algorithms to optimize laser parameters to improve (or set) electrochemical properties of supercapacitor. in this chapter, the short definition of selected

ML algorithms will be described, then data collection and preparation will be given in next part. Finally, we will analyze these three methods and will combine them to offer an inverse engineering strategy to get initial laser parameters to prepare specific electrodes.

4.2 Optimization Techniques

4.2.1 Logistic regression [110, 111]

Regression analysis is a form of the statistical process used to predict the relationships between a dependent variable (often referred to as the 'outcome' or 'response' variable) and one or more independent variables (often referred to as 'predictors,' 'covariates,' 'explanatory variables,' or 'features'). The most popular type of regression analysis is logistic regression, which involves determining the line (or a more sophisticated linear combination) that best fits the data-dependent on a certain mathematical criterion. The ordinary least squares approach, for example, computes the unique line (or hyperplane) that minimizes the sum of squared differences between the genuine data and that line (or hyperplane). This allows the scientists to predict the conditional expectation (or average population value) of the dependent variable when the independent variables take on a specified set of values for precise mathematical reasons. Less prevalent types of regression employ somewhat different approaches to estimate alternative location parameters (e.g., quantile regression or Necessary Condition Analysis) or the conditional expectation over a larger set of non-linear models (e.g., nonparametric regression). Regression analysis is generally employed for two fundamentally separate reasons. First, regression analysis is commonly used for prediction and forecasting, where it overlaps significantly with the subject of machine learning. Second, in some cases, regression analysis may be used to establish causal links between independent and dependent variables.

Researchers first choose a model to estimate and then use their preferred approach (e.g., ordinary least squares) to estimate the model's parameters. The following elements are included in regression models:

1. The unknown parameters are frequently denoted as a scalar or vector display style beta.
2. The independent variables seen in data are commonly expressed as a vector display style X_i (where display style ii specifies a row of data).
3. The dependent variable, which is seen in data and is frequently expressed by the scalar display Y_i.
4. The error terms are not immediately noticed in data and are frequently expressed by the scalar display style e_i.

Different terminologies are used in diverse domains of application in place of dependent and independent variables. Most regression models argue that display style Y_i is a function of display style X_i and display style beta, with display style e_i being an additive error component that might reflect un-modeled determinants of display Y_i or random statistical noise:

$$Y_i = f(X_i, \beta) + e_i \qquad 5.1$$

4.2.2 Support Vector Machine (SVM) [112, 113]

A Support Vector Machine (SVM) is a discriminative classifier described formally by a separating hyperplane. Put another way, given labeled training data (supervised learning), the algorithm generates an ideal hyperplane that categorizes fresh samples. In two

dimensions, a hyperplane is a line that divides a plane into two sections, with each class lying on each side.

SVM's training involves solving a Quadratic Program (QP) with linear constraints that depend on the training vectors, on a few kernel parameters, and on the separation margin limits. The QP solution provides the necessary information to choose, among all data, the most important vectors which define the separation hyper-plane between the classes, known as support vectors (SV). Since its formal description, support vector machines have been applied to several regression and classification problems. It has become a useful tool in pattern recognition, with applications in many areas like material categorization.

SVMs, as a first approximation, find a separation line (or hyperplane) between data of two classes. SVM is an algorithm that takes data as input and generates a line that, if possible, divides those classes.

4.2.3 Neural network [114-116]

A basic neural network has an input layer, an output (or target) layer, and a hidden layer in between. The layers are linked together by nodes, which create a "network" which is the neural network of interconnected nodes. A node is similar to a neuron in the human brain. However, if more than one perceptron is present and stacked together, we have created a neural network. The first layer's output becomes the input for the second layer until the output layer totals the total activation. The overall activation represents the network's confidence in its final choice. The input layer is the network's beginning point. This layer receives the values that will be utilized in the prediction. The network's "magic" is performed in the hidden layer. Throughout this region, the activation levels of the input

values are computed. The hidden layer might be as few or as many as required for the project. Finally, the activation of each of the final nodes is utilized to pick a solution in the output layer.

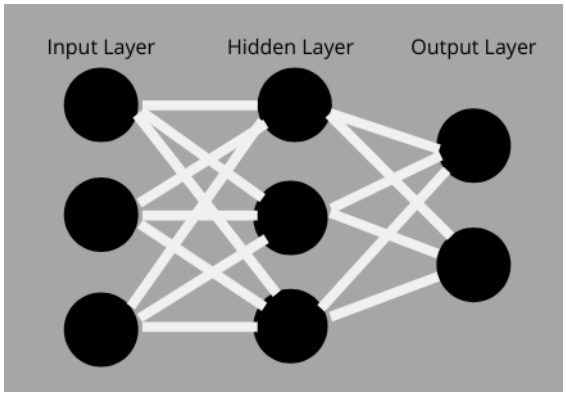

Fig 4.1 Neural Network Layers

As you can see, each unit is linked to each unit in the following layer. This enables neighboring perceptron’s to converse with one another and generate weights that are ideal for their usage.

Neural networks learn in two stages: feedforward (which we have already discussed) and backpropagation. Backpropagation may be divided into two steps: estimating the cost and then minimizing the cost. The cost is the difference between the network's anticipated value and the dataset's predicted value. The bigger the expense, the larger the inaccuracy. The objective is to keep costs as low as feasible. The key to accomplishing this is to reduce costs by adjusting weights and biases. Simply said, it is feedforward in reverse. We use matrix multiplication to change the weights so that some neurons get more attention based on what they'll be getting. Gradient descent is a typical approach for reducing the cost function. The aim is to discover the function's global cost minimum by adding up all the differences between the actual and predicted output and multiplying it by the learning rate. Mean-Squared Error is the most used cost function.

$$J(\Theta) = \frac{1}{m}\sum_{i=1}^{m}\left(h_\Theta\left(x^{(i)}\right) - y^i\right)^2 \qquad 5.2$$

The $J(\Theta)$ is called from the gradient descent function.

The learning rate, α, is essentially how large of a step to convergence to take (another way saying finding the global minimum). As an example, imagine you are standing on top of a hill with a beautiful valley below you. You begin to make your way down the hillside. Fighting the impulse to listen to your inner kid and roll down the hill quickly (perhaps missing your objective), you take your time and step easily down, avoiding any stones and sidestepping any trees in your path. The learning pace is comparable to the number of significant steps or ways required to reach the valley. If the learning rate is too fast, you may continue rolling up the opposite side and miss the valley altogether due to the momentum of your roll. If the learning rate is too slow, it will be dark before you reach the valley, which is the optimum aim. Finding the optimal learning rate for your model is critical for building a powerful and efficient neural network.

4.3 Data Set

4.3.1 Data collection

A systematic procedure of obtaining observations or measurements is known as data collection. Data collecting helps you to get first-hand expertise and unique insights into your study challenge, whether you are conducting research for industry, government, or academia. While techniques and goals may vary per field, the general data gathering procedure is usually the same. Also, we should think about the following things before starting to collect the data:

Table 4.I. Laser input parameters in the optimization process

	Variables	Description
Input	Frequency 1	Laser Frequency for electrode Fabrication
	Power 1	Laser Power for electrode Fabrication
	Pulse Duration 1	Laser PD for electrode Fabrication
	Scanning Speed 1	Laser SS for electrode Fabrication
	Frequency 2	Laser Frequency for electrode Fabrication
	Power 2	Laser Power for electrode Fabrication
	Pulse Duration 2	Laser PD for electrode Fabrication
	Scanning Speed 2	Laser SS for electrode Fabrication
Output	Specific Capacitance	Capacitance of electrode
	Charge/Discharge Retention	Retention of charge/discharge cycles
	CPE-P	Capacitance
	CPE-T	Reluctance
	R	Resistance

- The study's goal is to
- The sort of information you are gathering
- We employ the techniques and methods to acquire, store, and process data.

This section aims to find an equation that depicts the relation of laser parameters used in the fabrication process. In this section, we faced the pricy fabrication process of electrodes. In Machine learning problems, we need a large amount of data that can help us to find an optimum solution. In the fabrication process, generating a huge amount of data is pricey and time-consuming. For this reason, we decided to develop a small group of data and focus on the optimization algorithm to increase the accuracy of the results.

According to the laser variables in the fabrication process (power (P), frequency(F), pulse duration (PD), scanning speed (SS)), we prepared 21 different electrodes with a combination of laser parameters (Table 4.I). These 21 different electrodes and one raw sample provide 231 different supercapacitors for the next step. In the next step we gathered all fabricated electrode data by potentiostat machine. Before defining machine learning algorithms input, we had to classify data in different sections.

Table 4.II Sample parameters for electrode fabrication

	Frequency	Pulse Duration	Power	Scanning		Frequency	Pulse Duration	Power	Scanning
1	*600*	*pd1*	*15*	*100*	**12**	*1200*	*pd2*	*20*	*100*
2	*600*	*pd1*	*15*	*100*	**13**	*600*	*pd1*	*20*	*50*
3	*600*	*pd2*	*15*	*50*	**14**	*600*	*pd1*	*20*	*100*
4	*600*	*pd2*	*15*	*50*	**15**	*600*	*pd2*	*20*	*50*
5	*1200*	*pd1*	*15*	*50*	**16**	*600*	*pd2*	*20*	*100*
6	*1200*	*pd1*	*15*	*100*	**17**	*900*	*Pd1*	*15*	*50*
7	*1200*	*pd2*	*15*	*50*	**18**	*900*	*Pd2*	*15*	*50*
8	*1200*	*pd2*	*15*	*100*	**19**	*900*	*Pd1*	*10*	*50*
9	*1200*	*pd1*	*20*	*50*	**20**	*600*	*Pd1*	*10*	*50*
10	*1200*	*pd1*	*20*	*100*	**21**	*1200*	*Pd1*	*10*	*50*
11	*1200*	*pd2*	*20*	*50*	**22**	*0*	*0*	*0*	*0*

We divide fabrication, data collection, and optimization processes into three different phases. As it is shown in figure 5.2 in the first step, we applied the same fabrication process with PLA to generate our electrode. In phase II potentiostat helps us to gather all needed data, and finally, machine learning algorithms have been used to find the best relation between eight different laser parameters and two electrochemical outputs.

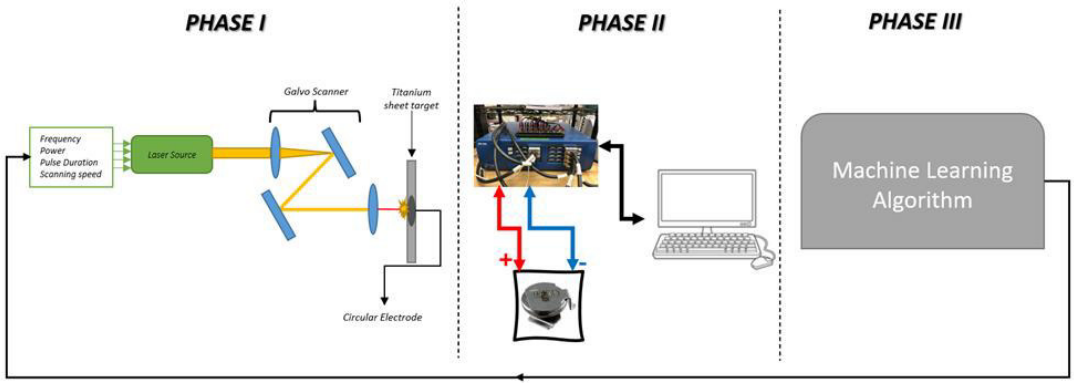

Fig 4.2 Inverse Engineering phasing

Considering the last research work, which analyzed electric storage material and fabrication process, in addition to our device technical abilities, we decided to choose two or three different values for each parameter. As we mentioned, frequency and power contain three different values, but pulse duration and scanning speed use two values. We

used logistic regression, support vector machine, and Neural Network. These results are partly due to the continuous use of machine learning algorithms in storage applications. These nominated algorithms have been used in different applications to generate predictive results in different concepts. We have compared the results of different ML algorithms in table III. As we can see, the prediction efficiency is best in the NN method, where the overall value is %84.83. The worst prediction efficiency is in Charge/discharge retention compared with other parameters.

Table 4.III Machin learning techniques prediction

	Capacitance	Resistance	CPE-P	CPE-T	Charge Retention
Logistic Regression	83.42	79.76	81.43	82.76	76.32
Support Vector Machine	84.43	81.23	83.45	84.32	74.56
Neural Network	86.56	86.34	86.45	86.47	78.34

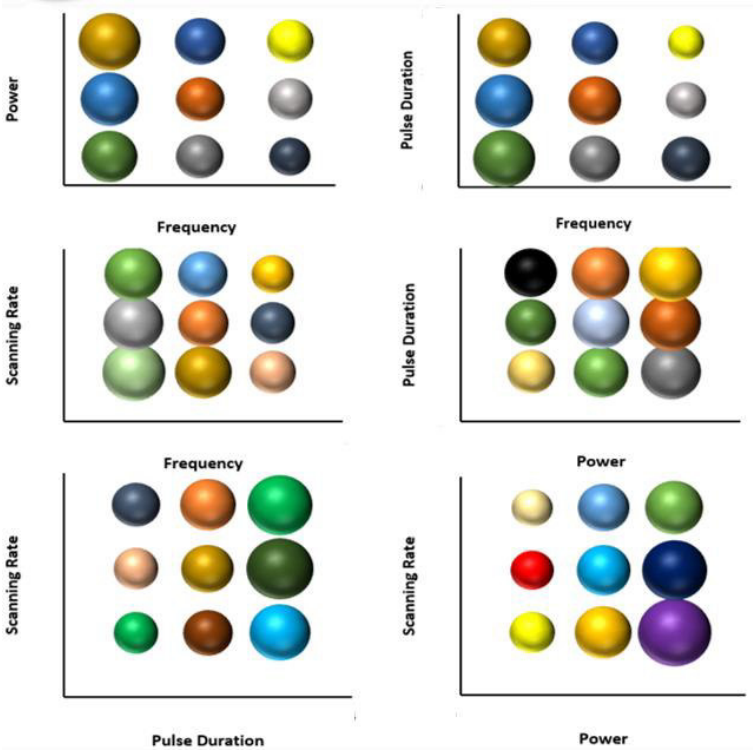

Fig 4.3 Comparison of independent parameter effect on C_{sp}

For comparing the relation between inputs and outputs, we used a bubble graph in figure 5.3. In figure 5.3-a, we can see the maximum capacitance could be obtained with minimum frequency and maximum power (frequency-power). Figure 5.3-b shows the relation of frequency-pulse duration with specific capacitance where minimum frequency and pulse duration can generate the best result. Figures 5.3-c to 5.3-f show the relation between generated capacitance and laser parameters. Figure 5.4 shows a Pareto graph comparing the number of supercapacitors in a specific capacitance horizon (black bar graphs) and accumulative number (orange linear graph). As we can see more than any bands, the fabricated supercapacitors are in middle bars and decreasing going to high and low capacitance. This graph shows the normal distribution of fabricated supercapacitors along with specific capacitance.

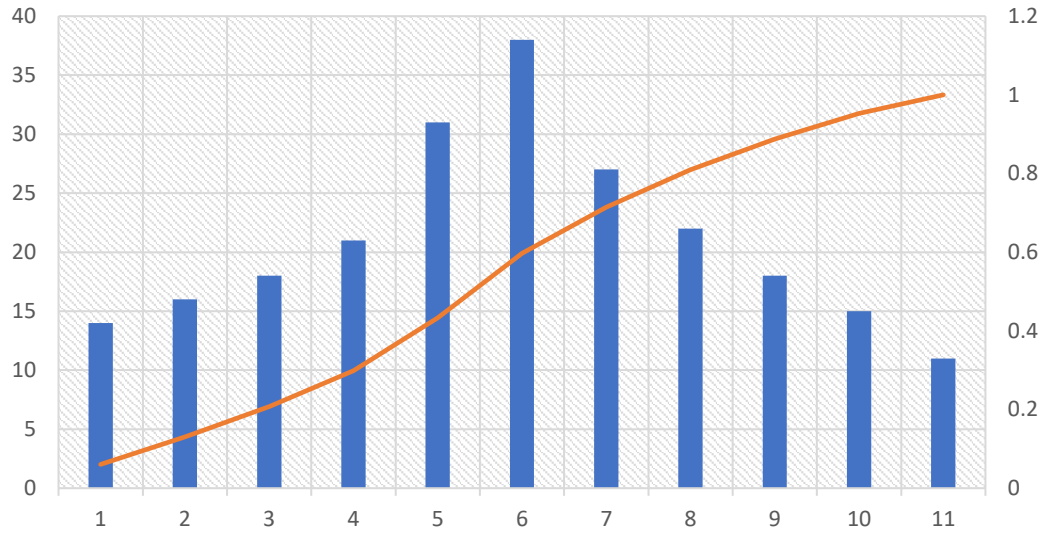

Fig 4.4 Distribution of C_{sp}

4.4 Inverse Engineering

Inverse methods are inverse engineering strategies which are used for the Parameter Estimation (PE) of a system or for its functional identification. In the former, the unknown

parameters can be estimated by means of experimental data. In the latter, the unknown parameters of laser can be determined in a finite or an infinite dimensional space. The solution methods for inverse problems are usually more complicated than direct problems, although direct problems are well-posed. The conditions that must be satisfied in a well-posed problem. As we know, the solution of most inverse problems is highly dependent on the initial condition, boundary conditions, and measured signals. There have been numerous attempts to tackle these difficulties and to convert inverse problems into well-posed problems. In the identification of the TiO_2 supercapacitor parameters, the time-varying cell potential value can be measured during the charge/discharge process. Also, other electrochemical parameters can be measured at the end of the test as input of our proposed system. Figure 4.5 illustrates the relationship between different elements of an Inverse Engineering (IE) study based on an inverse method. The objective functions are defined here as a couple of objectives on four main supercapacitor behaviors (C_{sp}, Resistance, CPE-P, and CPE-T) with N+m inequalities (N=2 and m=3). A number of inequalities in this optimization shows constraints on electrochemical properties. A mathematical optimizer is employed to minimize the objective function error to find the best values of the expected laser parameters.

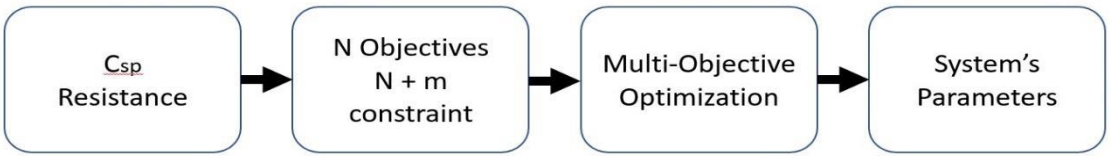

Fig 4.5 Inverse Engineering Flowchart

We accepted symmetrical supercapacitors in the optimization process, which includes the same electrode parameters. As we can see, we have a reasonable estimation of laser parameters for fabricating specific supercapacitors in our application. As an example, for

collecting C_{sp} = 0.806 m F/g laser parameters should be set according to this series (475 kHz, pd2, 12.3 W,63 mm/sec). We show more examples of specific capacitance in Table 4. IV.

Table 4. IV Inverse engineering parameter generation with specific C_{sp} and resistance

C_{sp}	Resistance	Frequency	Power	Pulse Duration	Scanning Speed
0.752	71.4	305	11	Pd2	52
0.800	78.4	481	10.4	Pd1	58
0.806	81.4	475	12.3	Pd2	63
0.853	85.3	708	12.4	Pd1	57
0.904	82.1	806	14.1	Pd1	71
0.996	68.4	901	17.3	Pd2	82
1.050	45.4	1100	18.3	Pd2	73
1.104	45.5	305	15.1	Pd2	71
1.154	55	541	16.3	Pd1	75
0.204	68.2	573	18.1	Pd2	79

Chapter 5. Conclusion

According to the last chapters, batteries excel at storing energy, while supercapacitors rate better for power. Although battery designers have been trying to combine these two energy storage devices to offer either more reliable or more efficient systems, different material-based projects to improve the energy density of supercapacitors are running at the same time. In this thesis, we tried to propose a new laser-based version of material preparation to recover the storage ability of titanium in supercapacitor structures in different applications. In this process, we based on the electrode surface structure to improve the functionality in electrical energy storage. Although increasing porosity accelerates more energy density in energy storage, other electrochemical properties changed in the opposite direction. In our experiments, the electrochemical properties of the supercapacitor have been analyzed by changing the electrode's porosity simultaneously.

Titanium, as a cheap, abundant, and durable material, has been selected for our project. We are hoping this talented material will be used in energy storage applications in the future. We did not focus on the other part of energy storage; however, we will try to define new projects to analyze them.

In chapter 5, we offered an inverse engineering method for optimal laser parameters. This method is based on the machine learning theory to optimize the electrochemical properties of supercapacitors. We can set four laser parameters using this method to get specific electrochemical properties in a supercapacitor.

Although supercapacitors can not be used as a single storage element (low energy density), many projects are trying to improve this weakness to substitute them in a battery application.

References

1. Maroto-Valer, M.M; Song, C; Soong, Y; Environmental challenges and greenhouse gas control for fossil fuel utilization in the 21st century, springer, 2002
2. Vaclav Smil, Energy Transitions: Global and National Perspectives, PRAEGE, 2016
3. Lodi, A; Frangioni, A; Selini, N; Hadjidimitriou; Koch, T, Mathematical Optimization for Efficient and Robust Energy Networks, Springer International Publishing, 2021
4. Rifkin, J; The Third Industrial Revolution, How Lateral Power Is Transforming Energy, the Economy, and the World, St. Martin's Publishing Group, 2011
5. Aulice Scibioh, M; Viswanathan, B, Materials for Supercapacitor Applications, Elsevier Science publication, 2011
6. Kularatna, N, Energy Storage Devices for Electronic Systems, Elsevier Science, 2014
7. Stevic, Z, New Generation of Electric Vehicles, IntechOpen, 2012
8. Venet, P; Redondo-Iglesias, E, Batteries and Supercapacitors Aging, MDPI AG, 2020
9. Bélanger, D; Qu, D; Long, J; Leonte, O.M; Kumta, P; Simon,P; Brousse, T, Electrochemical Capacitors: Fundamentals to Applications, Electrochemical Society, 2015
10. Sarkar, A.N; Diwan, P, Energy Security, Pentagon Energy Press

11. Afrakhteh. H; Gholami, A, Long term pump storage capacity planning for microgrid in model predictive control platform, 2016 24th Iranian Conference on Electrical Engineering (ICEE)
12. Michaelidesa, E; N.Michaelides, D, Impact of nuclear energy on fossil fuel substitution, Nuclear Engineering and Design Volume 366, September 2020
13. Gössling. S; Higham. J, The Low-Carbon Imperative: Destination Management under Urgent Climate Change, Journal of Travel Research, 2021
14. Kalair, A; Abas, N; Saleem, M.S; Kalair, A.R; Khan, N, Role of energy storage systems in energy transition from fossil fuels to renewables, Energy Storage, Volume3, Issue1, February 2021
15. Albertus, P; Girishkumar, G; McCloskey, B; Sánchez-Carrera, R; Kozinsky, B, Christensen, J; Luntz, AC, Identifying Capacity Limitations in the Li/Oxygen Battery Using Experiments and Modeling, Journal of The Electrochemical Society, Volume 158, Number 3, 2011
16. Koohi, S ; Rosen, MA, A Review of Energy Storage Types, Applications and Recent Development, Journal of Energy Storage, Elsevier, Volume 27, February 2020
17. Wang, Y; He, P; Zhou, H, A lithium–air capacitor–battery based on a hybrid electrolyte, Energy & Environmental Science, **2011**
18. Zhangab, L; Hucd, X; Wang, Z; Sun, F; Dorrellb, D, A review of supercapacitor modeling, estimation, and applications: A control/management perspective, Renewable and Sustainable Energy Reviews, Volume 81, Part 2, January **2018**

19. Devillers, N; Jemei, S; Péra, M; Bienaimé, D; Gustin, F, Review of characterization methods for supercapacitor modelling, Journal of Power Sources, Volume 246, 15 January **2014**, Pages 596-608
20. Zaharaddeen, I; Subramani, C; Dash, S, A Brief Review on Electrode Materials for Supercapacitor, Int. J. Electrochem. Sci., 11 (**2016**) 10628 – 10643
21. Qi, Z; Koenig, G, Review Article: Flow Battery Systems with Solid Electroactive Materials, Journal of Vacuum Science and Technology B: Nanotechnology and Microelectronics (JVSTB), 2017
22. Zhang, K; Han, X; Hu, Z; Zhang, X; Tao, Z; Chen, J, Nanostructured Mn-based oxides for electrochemical energy storage and conversion, Chemical Society Reviews, **2014**
23. Chena, K; Xue, D, Materials chemistry toward electrochemical energy storage, Journal of Materials Chemistry, **2016**
24. Peña-Alzola, R; Sebastián, R; Quesada, J; Colmenar, A, Review of flywheel-based energy storage systems, **2011** International Conference on Power Engineering, Energy and Electrical Drives
25. Jouhara, H; Żabnieńska-Góra, A; Khordehgah, N, Ahmad, D; Lipinski, T; Latent thermal energy storage technologies and applications: A review, International Journal of Thermofluids, Volumes 5–6, August **2020**, 100039
26. Kerskes, H; Mette, B; Bertsch, F; Asenbeck, S; Drück, H, Chemical energy storage using reversible solid/gas-reactions (CWS) – results of the research project, Energy Procedia, Volume 30, **2012**, Pages 294-304

27. Sagadevan, S; Johan, M; Marlinda, A; Akbarzadeh, O; Pandian, K; Shahid, MM; Mohammad, F; Podder, J, Chapter one - Background of energy storage, Advances in Supercapacitor and Supercapattery, An Innovation Toward Energy Storage Devices, **2021**, Pages 1-26
28. Zhang, J; Yang,Z; Lemmon, J; Imhoff, C; Graff, G; Liyu; et al, Materials Science and Materials Chemistry for Large Scale Electrochemical Energy Storage: From Transportation to Electrical Grid, Advanced Functional Materials, Volume23, Issue8, Special Issue: Grand Challenges in Energy Storage, **2012**
29. Wang, H; Yang, Y; Guo, Y, Nature-Inspired Electrochemical Energy-Storage Materials and Devices, Advanced Functional Materials, Volume7, Issue5, March 8, **2017**
30. Lv, W; Li, Z; Deng, Y; Yang, Q; Kang, F, Graphene-based materials for electrochemical energy storage devices: Opportunities and challenges, Energy Storage Materials, Volume 2, January **2016**, Pages 107-138
31. Fleischmann, S; Mitchell, J; Wang, R; Zhan, C; Jiang, D; Presser, V; Augustyn, V, Pseudocapacitance: From Fundamental Understanding to High Power Energy Storage Materials, Energy & Environmental Science, Issue 5, **2014**
32. B.Goodenough, J, Energy storage materials: A perspective, Energy Storage Materials, Volume 1, November **2015**, Pages 158-161
33. Rolison, D; Nazar, L, Electrochemical energy storage to power the 21st century, Cambridge University Press: 14 July **2011**

34. Luo, X; Wang, J; Dooner, M; Clarke, J, Overview of current development in electrical energy storage technologies and the application potential in power system operation, Applied Energy, Volume 137, 1 January **2015**, Pages 511-536
35. Roberts, B; Sandberg, C, The Role of Energy Storage in Development of Smart Grids, Proceedings of the IEEE, Volume 99, Issue 6, June **2011**
36. Baker, J, New technology and possible advances in energy storage, Energy Policy, Volume 36, Issue 12, December **2008**, Pages 4368-4373
37. Mahlia, T; Saktisahdan, T; Jannifar, A; Hasan, M; Matseelar, H, Renewable and Sustainable Energy Reviews, Volume 33, May **2014**, Pages 532-545
38. Zhao, X; Jiaqiang, E; Wu, G; Deng, Y; Han, D; Zhang, B; Zhang, Z, A review of studies using graphenes in energy conversion, energy storage and heat transfer development, Energy Conversion and Management, Volume 184, 15 March **2019**, Pages 581-599
39. Tamme, R; Taut, U; Streuberc, C; Kalfa, H, Energy storage development for solar thermal processes, Solar Energy Materials, Volume 24, Issues 1–4, 2 December 1991, Pages 386-396
40. Strielkowski, W; Lisin, E; Tvaronavičienė, M, TOWARDS ENERGY SECURITY: SUSTAINABLE DEVELOPMENT OF ELECTRICAL ENERGY STORAGE, Journal of Security & Sustainability Issues. **2016**, Vol. 6 Issue 2, p235-244. 10p.
41. Electrical energy storage, Electrical Energy Storage, Conference Report, Volume 12, Issue 4, August **1998**, p. 177 – 181

42. Hameer, S; van Niekerk, J, International Journal of Energy Research, February **2015**

43. Liu, K; Wang, Y; Lai, X, Introduction to Battery Full-Lifespan Management, MDPI, Data Science-Based Full-lifespan Management of Lithium-ion Battery **2022**

44. Kanakasabapathy, S, Large scale electrical energy storage systems in India-current status and future prospects, Journal of Energy Storage, Volume 18, August 2018, Pages 112-120

45. Ferreira, H; Grade, R; Kling, W; Lopes, J, Characterisation of electrical energy storage technologies, Energy, Volume 53, 1 May **2013**, Pages 288-298

46. Dréau, J.L; Heiselberg, P, Energy flexibility of residential buildings using short term heat storage in the thermal mass, Energy, Volume 111, 15 September 2016, Pages 991-1002

47. Lizana, J; Friedrich, D; Renaldi, R; Chacartegui, R, Energy flexible building through smart demand-side management and latent heat storage, Applied Energy, Volume 230, 15 November **2018**, Pages 471-485

48. Cunha, J; Eames, P, Thermal energy storage for low and medium temperature applications using phase change materials – A review, Applied Energy, Volume 177, 1 September **2016**, Pages 227-238

49. Chen, Q; Wang, Y, Research Status and Development Trend of Concentrating Solar Power, **2020** 9th International Conference on Renewable Energy Research and Application (ICRERA)

50. Fu, L.J; Liu, H; Li, C; Wu, Y.P; Rahm, E, Holze, R; Wu, H.Q, Electrode materials for lithium secondary batteries prepared by sol–gel methods, Progress in Materials Science, Volume 50, Issue 7, September **2005**, Pages 881-928
51. Sagadevan, S; Johan, M; Marlinda, A; Akbarzadeh, O; Pandian, K, Chapter one-Background of Energy Storage, Advanced in Supercapacitor and Supercapattery, An innovation Toward Energy Storage Devices, 2021
52. Sun, H, Zhu, G; Xu, X; Liao, M; Li, Y; Angell, M; Gu, M; Zhu, Y; Hung, W; Li, J, A safe and non-flammable sodium metal battery based on an ionic liquid electrolyte, Nature Communication, **2019**
53. Schupbach, R.M; Balda, J.C; Zolot, M; Kramer, B, Design methodology of a combined battery-ultracapacitor energy storage unit for vehicle power management, IEEE 34th Annual Conference on Power Electronics Specialist, **2003**. PESC '03.
54. Ogunniyi, E.O; Pienaar, H, Overview of battery energy storage system advancement for renewable (photovoltaic) energy applications, **2017** International Conference on the Domestic Use of Energy (DUE)
55. Portet. C, Simon. P.L; Flahaut, E; Laberty-Robert, C, High power density electrodes for Carbon supercapacitor applications, Electrochimica Acta, Volume 50, Issue 20, 25 July **2005**, Pages 4174-4181
56. Wang, S; Wei, T; Qi, Z, Supercapacitor Energy Storage Technology and its Application in Renewable Energy Power Generation System, Proceedings of ISES World Congress **2007** (Vol. I – Vol. V) pp 2805-2809

57. Kato, Y, CHEMICAL ENERGY CONVERSION TECHNOLOGIES FOR EFFICIENT ENERGY USE, Thermal Energy Storage for Sustainable Energy Consumption pp 377-391. **2007**

58. Gómez, F, Efficiency and economics of proton exchange membrane (PEM) fuel cells, International Journal of Hydrogen Energy, Volume 22, Issues 10–11,**1997**, Pages 1027-1037

59. SooKim, H; Abbas, M.A; SeokKang, M; Kyung, H; HoBang, J; CheolYoo, W, Study of the structure-properties relations of carbon spheres affecting electrochemical performances of EDLCs, Electrochimica Acta, Volume 304, 1 May **2019**, Pages 210-220

60. Stewart, S; Srinivasan, V; Newman, J, Modeling the Performance of Lithium-Ion Batteries and Capacitors during Hybrid-Electric-Vehicle Operation, Journal of The Electrochemical Society, Volume 155, Number 9, **2008**

61. Choudhary, N; Li, C; Moore, J; Nagaiah, N; Zhai, L; Jung, Y; Thomas, J, Asymmetric Supercapacitor Electrodes and Devices, Advanced Materials, Volume29, Issue21, June 6, **2017**

62. Kötz, R; Carlen, M, Principles and applications of electrochemical capacitors, Electrochimica Acta, Volume 45, Issues 15–16, 3 May **2000**, Pages 2483-2498

63. Wang, Y; Song, Y; Xia, Y, Electrochemical capacitors: mechanism, materials, systems, characterization and applications, Chemical Society Reviews, Issue 21, **2016**

64. Simon, P; Gogotsi, Y, Materials for electrochemical capacitors, Nanoscience and Technology, pp. 320-329, **2009**

65. Simon, P; Gogotsi, Y, Perspectives for electrochemical capacitors and related devices, Nature Materials volume 19, pages1151–1163, **2020**

66. Zhao, J; F.Burke, A, Electrochemical capacitors: Materials, technologies and performance, Energy Storage Materials, Volume 36, April **2021**, Pages 31-55

67. Sagadevan, S; Marlinda, A.R; Chowdhury, Z; et al, Chapter two-Fundamental Electrochemical Energy Storage System, Supercapattery **2021**

68. Liu, N; Ru, C; Wan, Q, Recent Advances in Electric-Double-Layer Transistors for Bio-Chemical Sensing Applications, MDPI, Sensors, 19(15), **2015**

69. Double Layer Capacitance, Wikipedia

70. Conway. B.E; Pell, W.G, Double-layer and pseudocapacitance types of electrochemical capacitors and their applications to the development of hybrid devices, Journal of Solid State Electrochemistry volume 7, pages637–644, **2003**

71. Li, N; Zhang, F; Tang, Y, Hierarchical T-Nb2O5 nanostructure with hybrid mechanisms of intercalation and pseudocapacitance for potassium storage and high-performance potassium dual-ion batteries, Journal of Materials Chemistry A, Issue 37, **2018**

72. Costentin, C; Savéant, J, Energy storage: pseudocapacitance in prospect, Chem. Sci., **2019**, **10**, 5656-5666

73. Augustyn, V; Come, J; Lowe, M; Kim, J; Taberna, K; Tolbert, S; Abruña, H; Simon, P; and Dunn, B, High-rate electrochemical energy storage through Li+ intercalation pseudocapacitance, Nature Materials, 12, pages518–522, **2013**

74. Li, J; Yuan, X; Lin, C; Yang, Y; Xu, L; Du, X; Xie, J; Lin, J; Sun, J, Achieving High Pseudocapacitance of 2D Titanium Carbide (MXene) by Cation

Intercalation and Surface Modification, Advanced Energy Materials, Volume7, Issue15, August 9, **2017**

75. Lee, Y; Chang, J; Hu, C, Differentiate the pseudocapacitance and double-layer capacitance contributions for nitrogen-doped reduced graphene oxide in acidic and alkaline electrolytes, Journal of Power Sources, Volume 227, **2013**, Pages 300-308,
76. Moghareh Abed, M; Gaspari, F; Kiani, A, Optical properties of Si/SiO2 nano structured films induced by laser plasma ionization deposition, Optics Communications, Volume 462, **2020**, 125297
77. Moghareh Abed, M; Kiani, A; Optical reflectivity of heat-treated nanofibrous silicon thin-films induced by high energy picosecond laser pulses, Sensing and Bio-Sensing Research, Volume 30, December 2020
78. Tan, C; Zhou, K; Ma, W; Attard, B; Zhang, P, Selective Laser Melting of High-Performance Pure Tungsten: Parameter Design, Densification Behavior and Mechanical Properties, Science and technology of Advanced Material, Volume 19- Issue 1, **2018**
79. Moghareh Abed, M; Investigation of selective optical properties of Si/SiO2 nanostructures generated by pulsed laser ablation as-deposited and post-treated, Ontario Tech University thesis, **2020**
80. Basic Overview of the Working Principle of a Potentiostat/galvanostat (PGSTAT)-electrochemical Cell Setup, Metrohm Autolab B. V. , Autolab Application Note EC08

81. Nam, K; Choi, G; Kim, H; Yoo, M; A Potential Readout Circuit with a Low-Noise and Mismatch-Tolerant Current Mirror Using Chopper Stabilization and Dynamic Element Matching for Electrochemical Sensors, **2021** MDPI, Applied Science

82. Lewczuk,B; Szyryńska, N; Field-Emission Scanning Electron Microscope as a Tool for Large-Area and Large-Volume Ultrastructural Studies, MDPI, Animals **2021**, 11(12), 3390

83. Mohammed, A; Abdullah, A; Scanning Electron Microscopy (SEM): A Review, Proceedings of **2018** International Conference on Hydraulics and Pneumatics

84. Copeland, L and Bragg, R; Quantitative X-Ray Diffraction Analysis, ACS Publications, **1958**

85. Whittig, L; Allardice, W; X-Ray Diffraction Techniques, Methods of Soil Analysis: Part 1 Physical and Mineralogical Methods, 5.1, Second Edition

86. Ameh, E; A review of basic crystallography and x-ray diffraction applications, The International Journal of Advanced Manufacturing Technology volume 105, pages3289–3302, **2019**

87. Velásquez, P; Leinen, D; Pascual, J; Ramos-Barrado, J; Grez, P; Gómez, H; Schrebler, R; Del Río, R; and Córdova, R; A Chemical, Morphological, and Electrochemical (XPS, SEM/EDX, CV, and EIS) Analysis of Electrochemically Modified Electrode Surfaces of Natural Chalcopyrite (CuFeS2) and Pyrite (FeS2) in Alkaline Solutions, The Journal of Physical Chemistry B, **2005**

88. Randviir, E; Metters, J; Stainton, J; and Banks, C; Electrochemical impedance spectroscopy versus cyclic voltammetry for the electroanalytical sensing of

capsaicin utilising screen printed carbon nanotube electrodes, Analyst, Issue 10, **2013**

89. Gharbi, O; T.T.Tran, M; Tribollet, B; Turmine, M; Vivier, V; Revisiting cyclic voltammetry and electrochemical impedance spectroscopy analysis for capacitance measurements, Electrochimica Acta, Volume 343, 20 May **2020**
90. Lee, J; Electrochemical Sensing of Oxygen gas in ionic liquids on Screen printed Electrodes, Curtin University thesis, **2014**
91. Anuradha, J; Cyclic Voltammetry: Principle, Instrumentation & Applications, Slideshare.net
92. Testing Electrochemical Capacitors, Gamry Instruments
93. Gholami, A.H; Kiani, A; Laser-induced nanofibrous titania film electrode: A new approach for energy storage materials, Journal of Energy Storage 31, 101654, **2020**
94. Gholami, A; Yim, CH; Kiani, A; Electrochemical Performance of Titania 3D Nanonetwork Electrodes Induced by Pulse Ionization at Varied Pulse Repetitions, Nanomaterials 11 (5), 1062, **2020**
95. Gholami, A; Kiani, A; New Generation of Tio2 Electrode in Supercapacitor, Proceedings of the 5th International Conference on Theoretical and Applied Nanoscience and Nanotechnology (TANN), **2021**
96. Luca, D; Macovel, D; and Teodorescu, CD; Characterization of titania thin films prepared by reactive pulsed-laser ablation, Surface science, Surf. Science, **2006**

97. Takagi, H; Uchida, S; Kitazawa, K; and Tanaka, S; High-Tc Superconductivity of La-Ba-Cu Oxides. II. –Specification of the Superconducting Phase, Japanese Journal of Applied Physics, Volume 26, Number 2A, **1987**

98. Jiang, C; Hosono, E; Zhou, H; Nanomaterials for lithium-ion batteries, Volume 1, Issue 4, November **2006**, Pages 28-33

99. Suttiponparnit, K; Jiang, J; Sahu, M; Suvachittanont, S; Charinpanitkul, T; and Biswas, Role of Surface Area, Primary Particle Size, and Crystal Phase on Titanium Dioxide Nanoparticle Dispersion Properties, Nanoscale Res Lett volume 6, Article number: 27, **2011**

100. Patel, J; Tribological capabilities of carbon-based nano additives in liquid and semi-liquid lubricants, Ontario Tech thesis, **2019**

101. Vijayakumar, S; Lee, S.H; Ryu, K.S; Hierarchical CuCo2O4 nanobelts as a supercapacitor electrode with high areal and specific capacitance, Electrochimica Acta, Volume 182, 10 November **2015**

102. Zhang, W.; Xu, J.; Hou, D.; Yin, J.; Liu, D.; He, Y.; Lin, H; Hierarchical porous carbon prepared from biomass through a facile method for supercapacitor applications, J. Colloid Interface Sci. **2018**, 530, 338–344

103. Taer, E.; Apriwandi, A.; Dalimunthe, B.K.L.; Taslim, R., A rod-like mesoporous carbon derived from agro-industrial cassava petiole waste for supercapacitor application, Chem. Technol. Biotechnol. **2021**, 96, 662–671

104. Haetge, J; Hartmann, P; Brezesinski, K; Janek, J; Ordered Large-Pore Mesoporous $Li_4Ti_5O_{12}$ Spinel Thin Film Electrodes with Nanocrystalline

Framework for High Rate Rechargeable Lithium Batteries: Relationships among, Chem. Mater. **2011**, 23, 19, 4384–4393

105. Young, C; Park, T; Woo Yi, J; Kim, J, Hossain, S; Kaneti, Y; Yamauchi, Y; Advanced Functional Carbons and Their Hybrid Nanoarchitectures towards Supercapacitor Applications, Chemistry A European Journal, Volume11, Issue20, October 24, **2018**

106. Fletcher, S.; Black, V.J.; Kirkpatrick, I; A universal equivalent circuit for carbon-based supercapacitors, Solid State Electrochem. **2014**, 18, 1377–1387.

107. Gönüllü, Y.; Kelm, K.; Mathur, S.; Saruhan, B, Equivalent circuit models for determination of the relation between the sensing behavior and properties of undoped/cr doped TiO2 NTs, Chemosensors 2014, 2, 69–84, **2014**

108. Rose, K; Deterministic annealing for clustering, compression, classification, regression, and related optimization problems, Proceedings of the IEEE, Volume: 86, Issue: 11, Nov **1998**

109. Xue, R; Wu, Z; A Survey of Application and Classification on Teaching-Learning-Based Optimization Algorithm, IEEE Access, Volume 8, **2019**

110. Kleinbaum, D; Klein, M; Logistic Regression, Springer, ISBN: 978-1-4419-1742-3, **2002**

111. Stoltzfus, J; Logistic Regression: A Brief Primer, Academic Emergency Medicine, Volume18, Issue10, October **2011**, Pages 1099-1104

112. A.Pisner, D; M.Schnyer, D; Chapter 6 - Support vector machine, Machine Learning, Methods and Applications to Brain Disorders, **2020**, Pages 101-121

113. Cervantes, J; Garcia-Lamont, F; Rodríguez-Mazahua, L; Lopez, A; A comprehensive survey on support vector machine classification: Applications, challenges and trends, Neurocomputing, Volume 408, 30 September **2020**, Pages 189-215

114. Bashar, A; SURVEY ON EVOLVING DEEP LEARNING NEURAL NETWORK ARCHITECTURES, Journal of Artificial Intelligence and Capsule Networks, **2019**

115. Albawi, S; Mohammed, T.A; Al-Zawi, S; Understanding of a convolutional neural network, **2017** International Conference on Engineering and Technology (ICET)

116. Zhang, Z; Artificial Neural Network, Multivariate Time Series Analysis in Climate and Environmental Research pp 1-35, **2018**